



**UNIVERSIDADE
DE VIGO**



**University of Chemical
Technology and Metallurgy**

**COMPARATIVE RESEARCH OVER
HYBRID AND HYBRID NANO-
COMPOSITE PROTECTIVE PRIMARY
COATINGS FOR AIRCRAFT ALLOY
AA2024 - T354**

HEAD OF DEPARTMENT: Assoc. Prof. Dr. Eng. Stoyan Dzhambazov.....

SUPERVISOR: Prof. Dr. Sc. Eng. Vladimir Kozhukharov.....

TUTOR: Dipl. Eng. Stephan Kozhukharov

REFEREE:

AUTHOR: Aberto Areal Salve.....

Sofia . April 2011

ACKNOWLEDGEMENTS

The author thanks and highly appreciated the financial supports from EC– ERSMUS office and from the Bulgarian NSF, contract DVU-02/102. The author is grateful to Dr. S. Kozhukharov, Assoc. Prof. Dr. M. Machkova, Assoc. Prof. Dr. I. Nenov and Prof. DSc. Dr. Vl. Kozhukharov, all from UCTM- Sofia, all from LAMAR team, for the useful discussion done.

CONTENTS

	page
I. THEORETICAL PART	
1. Introduction	
1.1. Nature of the corrosion processes	5
1.2. Classification of the standard aluminium alloys.....	8
1.3. Description of the hybrid nano-composite materials, and the corresponding technologies applied.....	9
1.4. Hybrid primer coatings – basic concepts and definitions.....	18
1.5. Concepts for active and passive corrosion protection.....	24
1.6. Hybrid nano-composite primer coatings. Basic concepts.....	24
1.7. Mechanism of the inhibitive effect of the lanthanide's compounds on the corrosion processes.....	27
1.8. Technologic features of the production of hybrid nano-composite primer coatings.....	30
1.9. Alternatives for the self healing coatings containing inhibitors.....	31
1.10. Basic concepts and definitions related to the Electrochemical Impedance Spectroscopy.....	34
1.11. Electrochemical impedance and impedance modeling.....	38
1.12. Practice in the electrochemical impedance spectroscopy.....	43
1.13. Topographic observations and description of the surface.....	44
2. Aims of the study.....	48
II. EXPERIMENTAL	
1. Objects of research	
1.1. Influence of the inhibitor's addition to hybrid primary coatings.....	49
1.2. Electrochemical systems with coated aluminium plates.....	49
2. Materials and methods	
2.1. Preparation of hybrid nano-composite coatings.....	50
2.2. Brief description of the measuring procedure.....	51
2.3. Topographic observations.....	53

III. RESULTS AND DISCUSSIONS

1. Model equivalent circuits used for fitting of the spectra

1.1. Equivalent circuit applied for description of the systems of direct addition of corrosion inhibitor into the corrosive medium.....54

2. Results obtained after fitting of the experimental data to the appropriated equivalent circuits

2.1. Results for sample with 2% CeCl₃.....57

2.2. Results for sample with 4% CeCl₃.....59

2.3. Results for sample with 2% CeCl₃ preliminary incorporated in 8% Al₂O₃ nano-particles.....61

2.4. Results for sample with 4% CeCl₃ preliminary incorporated in 8% Al₂O₃ nano-particles.....64

IV. DISCUSSION ABOUT THE RESULTS OBTAINED BY MODELING

1. Discussions over the evolution of the impedance parameters for the hybrid primer coatings.....67

2. Discussions over the evolution of the impedance parameters for the hybrid nano-composite primer coatings.....69

3. Protective ability of the hybrid and the hybrid nano-composite coatings.....70

4. Surface morphologic observations of the coatings by AFM.....74

4.1. Topographic surface observations.....74

4.2. Quantitative evaluation of the surface roughness.....76

V. CONCLUCIONS.....78

VI.REFERENCES.....80

I. THEORETICAL PART

1. Introduction:

1.1. Nature of the corrosion processes

It is well known, that the corrosion is destruction of the constructive materials, as consequence of their interactions with the surrounding environment. It could reveal at the either at surface, or in the bulk of the respective materials. The former one is rather consequence of chemical or electrochemical interactions with species, originated from the surrounding environment, while the latter is generally result from mechanical impact (known also as fatigue effect). The mechanical corrosion always reveals as structural changes, which lead to undesirable alterations of the properties of the corresponding materials, which lead to their disintegration.

Different approaches for classification of the corrosion could be found in the literature, according the nature of the destructive processes which composes it. Davis [1] suggests schematic presentation of the corrosion processes, as follows:

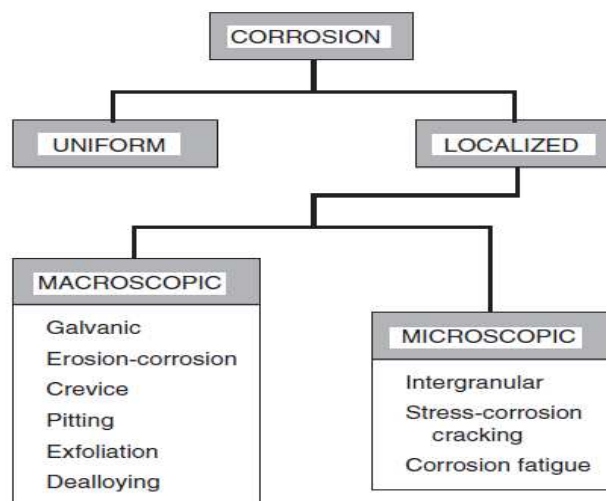


Figure 1. General Classification of the corrosion processes [1]

In addition, the same author has created a visual classification, which could be represented as follows:

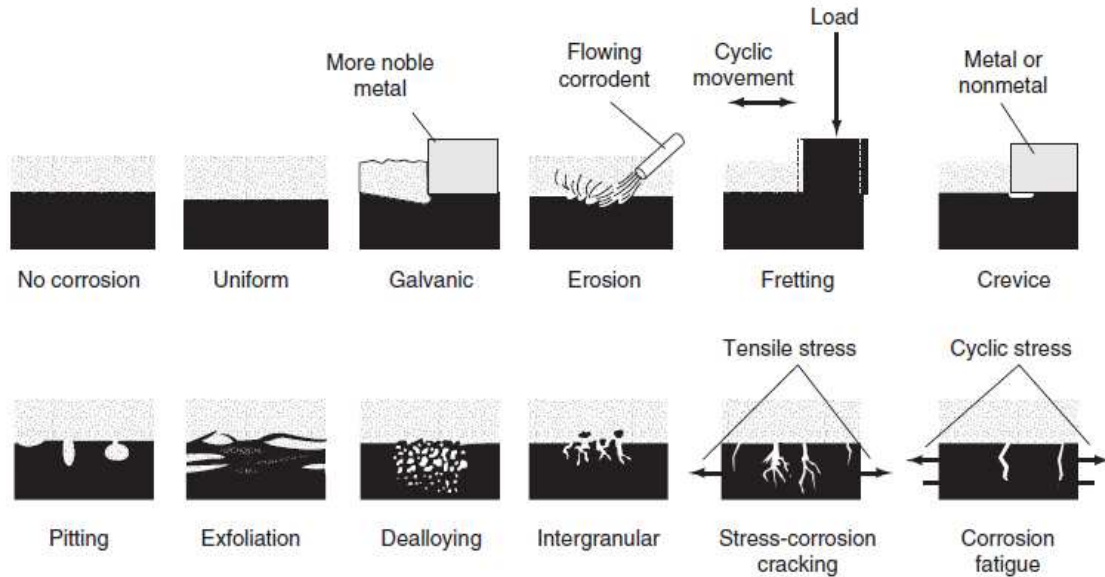


Figure 2. Schematic presentation of various mechanical and chemical kinds of corrosion

The chemical corrosion in the alloys possesses generally localized character. Its mechanism is predominantly electrochemical, due to simultaneous presence of more noble and more active metals. Thus, if a drop of electrolyte touches surface of given alloy, than immediately cathodic and anodic areas appear. The former belong to noble, and the anodic are originated by more active metals.

The electrochemical nature of the localized corrosion is predetermined by presence of cathodic areas where different reactions of reduction take place:

Oxygen reduction is represented in the electrolyte's solution:



Alternatively, hydrogen evolution is also possible:



On the anodic zones different oxidation processes pass, predominantly electrochemical dissolution of the active metal:



After comparison of reactions 1 – 3, it becomes obvious that addition or losing of electrons, which leads to respective changes of the oxidation rates of the respective reactants. These electrochemical processes pass simultaneously with electrons transfer from the anodic to the cathodic area, as it is clearly demonstrated in Figure 3:

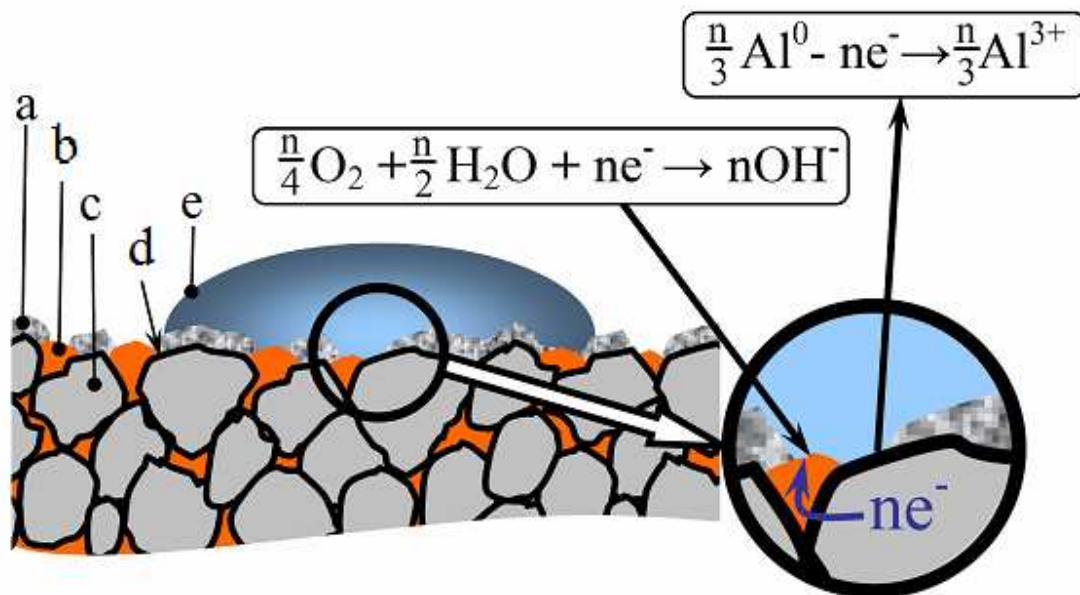


Figure 3. Illustration of electrochemical corrosion of Al-Cu alloy

a – Surface native oxide layer on the Al-anodic part; b – Copper inclusion; c – area of the aluminium matrix; d – surface boundary of the Aluminium part; e – drop of electrolyte (water solution of NaCl); magnification and reactions of e- transfer process

1.2. Classification of the standard aluminium alloys

In the industry there were various national standards, where the aluminium alloys possess special codes. In practice, it revealed the nominal compositions as well as the method applied for their metallurgic production and finishing treatments [2].

Nowadays, the industrial aluminium alloys have codes which are composed by the abbreviation “AA”, with addition of four digit numbers (NXXX), which reveal the composition of the alloy, as is shown in Table 1:

Table I. Codes of aluminium alloys vs. concentration of the main alloying element

Code of the Aluminium alloy (AA NAAA)	Concentration of the main alloying element
AA1XXX	99.0% minimum;
AA2XXX	Copper (1.9%...6.8%);
AA3XXX	Manganese (0.3%...1.5%);
AA4XXX	Silicon (3.6%...13.5%)
AA5XXX	Magnesium (0.5%...5.5%);
AA6XXX	Magnesium and Silicon (Mg 0.4%...1.5%, Si 0.2%...1.7%);
AA7XXX	Zinc (1%...8.2%);
AA8XXX	Others

In Table 1, the first digit (N) indicates the alloy group according to the major alloying element. The second digit indicates modification of the alloy or impurity limits. Usually, the original (basic) alloy is designated by “0” as the second digit. Numbers from 1 to 8 indicate various alloy modifications with slight differences in the compositions marked.

In the alloys of the 1XXX series the second digit indicates modifications in impurity limits: 0 means natural impurity limit, 1...8 indicate special control of one or more impurities or alloying element. **The last two digits** identify exact aluminum alloy or indicate the alloy purity level.

For example, AA1XXX = 1070 or 1170 that mean minimum 99.70% of aluminum in the alloys, 1050 or 1250 mean 99.50% of aluminum in the alloys, 1100 or 1200 mean minimum 99.00% of aluminum in the alloys.

In all other groups of aluminum alloys (2XXX through 8XXX) the last two digits signify different alloys in the group.

1.3. Description of the hybrid nano-composite materials, and the corresponding technology applied.

1.3.1. Needs for development of advanced corrosion protective systems

Aluminium is an important metal in industry owing to its specific characteristics. Hence, it is widely used as a material for automobiles, aviation, household articles and electronic devices [4], as well. For the needs of the aircraft industry the aluminum is used generally in form of alloys with improved mechanical properties, expressed generally by enhanced resistance to mechanical and atmospheric impact [5]. In the literature, [6] the Al – Cu (AA 2XXX) alloys are described to possess excellent weight to mechanical properties, which is the reason for their common use in the aeronautical industry for numerous structural components. Despite their apparent advantages, in a number of cases, the use of the aluminium alloys is limited by their aptitude to sufferer corrosion processes in aggressive environments [7]. On the other hand, the high content of variety alloying elements in the high strength Al-alloys promotes the generation of multiphase alloy system after appropriate thermomechanical treatment [8]. For such alloys, microgalvanic coupling between different metallurgical phases in presence of aggressive environments increases their susceptibility to localized corrosion. That is the reason for the pre-treatments by primer coatings of the metallic substrates in the industrial practice, before their application. Usually an organic paint is applied in order to improve adhesion between the polymer and the metal and to provide an additional long term corrosion protection, as well [7].

Rosero-Navarro [8] mentions that the typical protection systems involve various coating layers, including sol-gel or porous anodic films, organic primers (primer coatings) and top-coats, capable to provide specific active and/or passive corrosion protection. Concerning active protection, the presence of corrosion inhibitors is critical for protection of regions where damage of the multilayered system leads to direct exposure of bare alloy to aggressive environment. In this context, the Chromium Conversion Coatings (CCC) were used in the industrial practice during last decades, because of the inhibitive effect of Cr-species against the corrosion processes [8-11].

However, the chromium compounds have evinced to be carcinogenic and environmentally unacceptable contaminants. As result, the use of chromium has been banned since 2007 for corrosion protection in the automotive industry, by “End Life Vehicles“ (EVL) directive of EC. In addition, its application in the electronic industry was prohibited since 2006, by the “Restriction of Hazardous Substances” (RoHS) European directive [12].

On the other hand, the *sol-gel* approach for preparing of oxide protective films (coatings) has emerged as a versatile method [13]. Its application for effective corrosion protection of aluminium alloys is proposed by Hamdy and Butt [14].

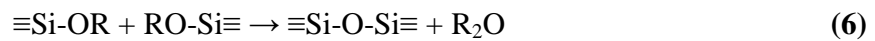
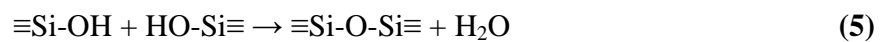
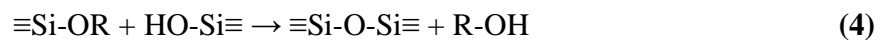
1.3.2. Basic concepts, related to the sol-gel approach

As it is already mentioned above, in the present text, the sol-gel approach is a versatile method, and it could be successfully used for corrosion protection of various alloys.

In addition to the emphasized by Hamdy and Butt [14] another advantages of the application of this method are the possibility for synthesis of advanced hybrid, and hybrid composite, and/or hybrid nano-composite materials, respectively. All of technologies, which include sol, or gel as intermediated stage, could be treated as technologies, based on the sol-gel approach. The **SOL** – could be assumed as a kind of colloidal system. The colloidal systems occupy intermediated place between real solutions, and rough (macroscopic) solutions, according the size of the particles of the dissolved fraction [15]. The approximated interval of the particle size of the dissolved

phase is between 1 and 1000nm. After the hydrolysis – polymerization processes is accomplished, described by the reactions (4-6), marked below, i.e. the corresponding sol converts to a gel product. According to the ref. [16, 17] the gels could be described as heterogeneous systems, where the liquid phase is involved into a solid polymeric matrix.

The basic manner for performance of the sol-gel approach is by mixing of one or more metal alkoxides with acid, in medium of alcohol. The metal alkoxides are metal-organic compounds which possess aptitude to hydrolyze in presence of acid. Afterwards, the obtained by the hydrolysis moieties joint themselves, resulting polymeric chains, and even branched matrixes. According to Dislich [18] chemically, the process could be described as follows:



Where “R” means whatever organic radical. In addition, Dislich demonstrates that compounds of more than 40 elements are used in the field of the sol gel technologies.

In laboratory conditions, the sol-gel approach could be performed by slow dropping of the corresponding alkoxide in alcohol (as is shown on figure x), and after addition of only few drops of acid (used as catalyses), the processes of hydrolysis and polymerization is going on. During these processes, the viscosity of the liquid media gradually increases. Afterwards, the system suffers solidification, obtaining form of a soft elastic solid body (namely, gel).

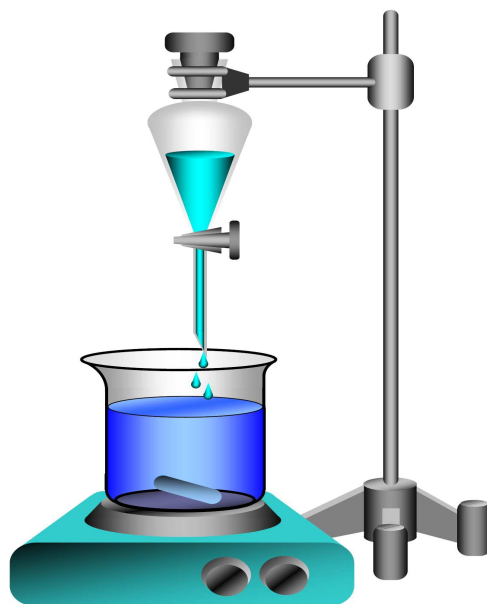


Figure 4. Laboratory system for synthesis via sol-gel route

By addition of supplementary organic or organo-metallic substance, for instance 3-glycidopropyltrimethoxysilane (GPTS) [19], or polydimethylsilyloxane (PDMS), [20], hybrid materials could be synthesized.

The **hybrid material** has intermediated position between purely organic, and completely inorganic substances. By that manner they are able to combine the typical features of both basic classes of substances. In this context, Zheludkevich [21] remarks that both parts of the hybrid primer coatings influence over the performance of the respective hybrid material: the inorganic components contribute to increase of the scratch resistance, durability and the adhesion to the metal substrate. The organic component increases density, flexibility and functional compatibility with the upper organic finishing paints. Further, in the literature [16], there is clear classification of the basic materials, as it is presented in the following Figure 5:

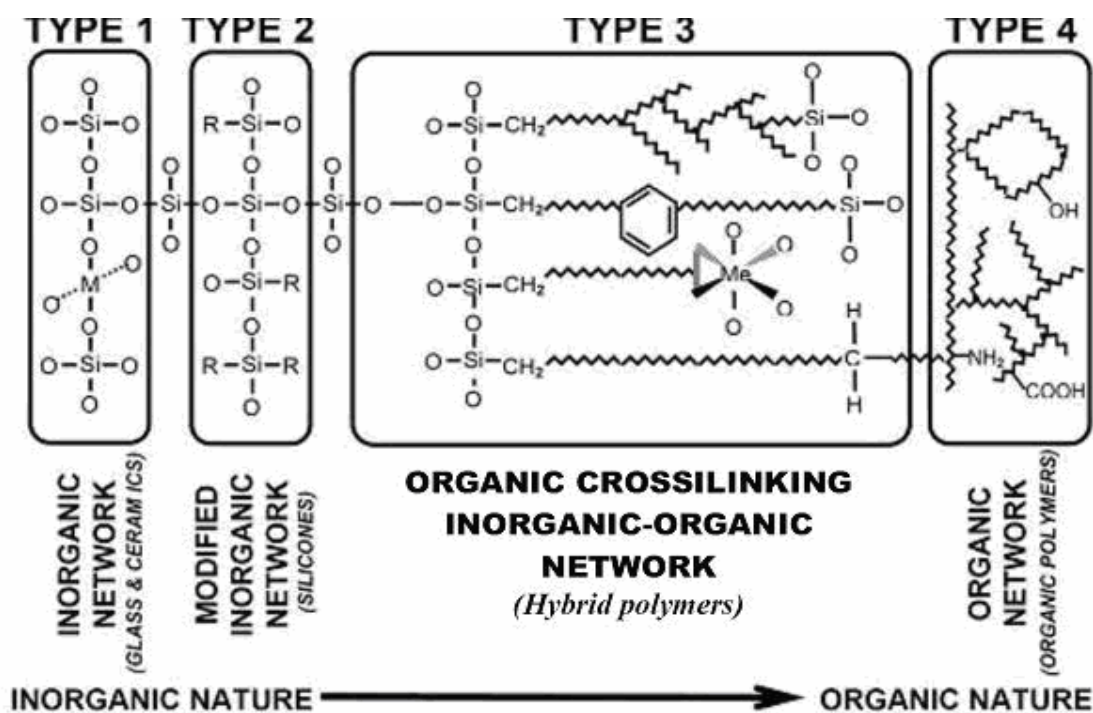


Figure 5. Basic classes for a hybrid network, according to their nature [22]

An additive improvement of the mechanical stability of the hybrid materials (especially primer coatings) could be achieved via introduction of nano-particles into the hybrid matrix. As a result, these particles could serve as reinforcing phase for the hybrid material [16, 22]. By application of this useful approach, completely new class of primer coatings could be produced. These materials are known as *hybrid nanocomposite primer coatings*.

1.3.3. Technologic bases of the sol-gel route.

During the recent years, the sol-gel method has found to be promising approach for development of large variety of advanced materials, which enable combinations of desirable properties. In practice, the method could be treated as basic one, for development of entire new generations of materials, and respectively anticorrosion coatings.

In this section, the basic definitions and concepts, related to the sol-gel synthesis will be a target for discussion. Usually, it is accepted that the condensed matter (liquids

Alternatively, valuable pharmaceutical products could be achieved via selective poly-peptisation of amino-acids at given pH of the medium, but this topic is not object of the present research.

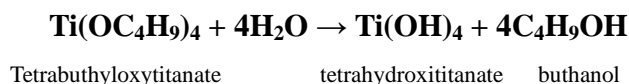
Hybrid and inorganic gel products could be synthesized via hydrolysis/polymerization processes of metal alkoxides. This class of substances is composed by molecules, consisted on organic moieties, connected via chemical bonds with metal oxide groups. In short, they possess a general formulae $(R-O)_nMe$, where “R” are organic radicals, “Me” is the corresponding metal ion, and “n” is the number of the organic radicals, and corresponds to the oxidation state of the metal ion. Here should be mentioned that there is a large diversity of different metal alkoxides. The name of given metal alkoxide depends on the metal, as well as the chemical composition of the organic radicals, connected with it. The most widely used Si- alkoxides are: Tetraethoxysilane, known also as Tetraethylorthosilicate (TEOS), and glycyloxipropyl trimethoxysilane (GPTS).

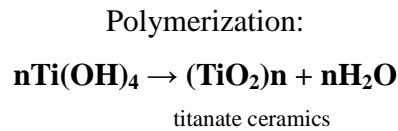
Here, the sol-gel synthesis is based on hydrolysis/polymerization processes of the corresponding alkoxides in liquid medium, represented by alcohol-water mixtures, in presence of acid. The last one is an initiator, and catalyst of the hydrolysis process. The activated via the hydrolysis active moieties react between themselves, obtaining a polymeric product, with enclosed, and uniformly distributed liquid phase in its bulk (chemical gel).

Besides the silicon, other metals also could be represented in the composition of the corresponding metal alkoxide. Kozhukharov et. al. [24] have synthesized light refractive coatings on glass substrates, composed by TiO_2 , by hydrolysis/polymerization of tetrabuthyloxitanate $Ti(OBu^n)_4$, and subsequent calcinations procedure of the hybrid gel product.

The chemical reactions could be described as follows:

Hydrolysis:





Similar processes are involved in the obtaining of hybrid primer coatings via sol-gel route.

The general scheme of the sequence of the technologic processes, related to the sol-gel route is represented in Figure 6:

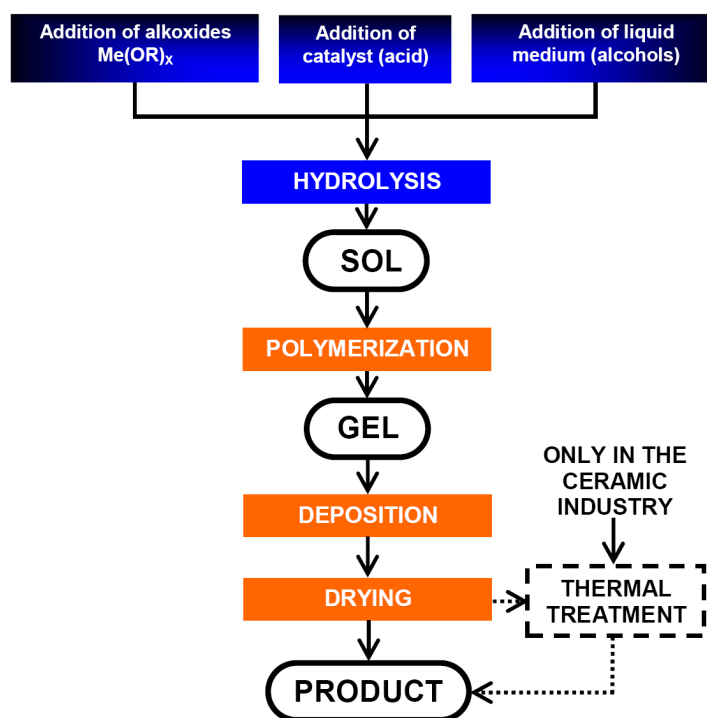


Figure 6. General schematic view of the technologies based on sol-gel route

Usually, the gel undergoes drying (annealing), in order to convert to desired end-product. If the desired product should be with completely inorganic composition, than the corresponding gel (as intermediated product), undergoes calcination process. During this posterior process, all of the organic bridge compounds burns, and only the inorganic part remains. Evidently is, that there is narrow relation between the structure and composition of the obtained products and the conjunction among composition of the precursors, the method and conditions applied for their synthesis. As is illustrated in Figure 7 [16].

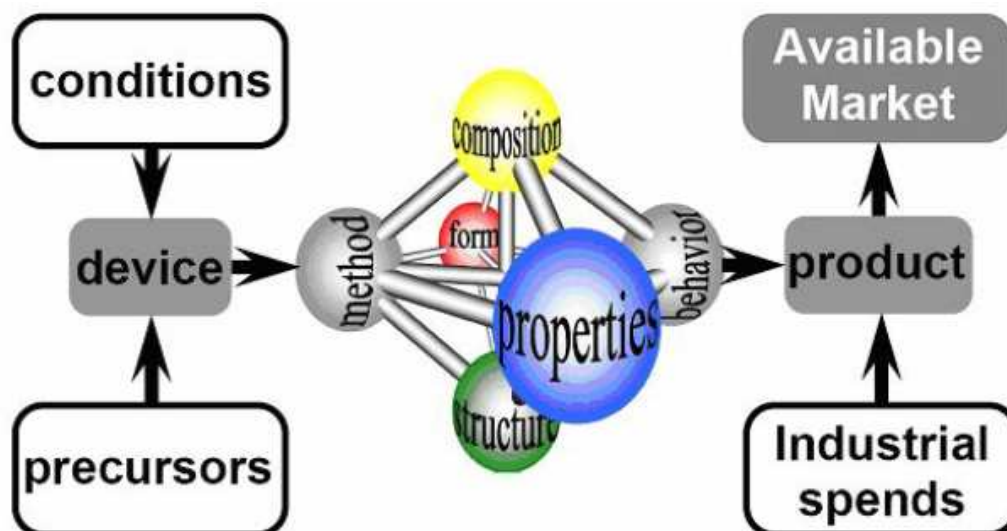


Figure 7. Relation between the applied conditions and the properties of the products

Namely in this article [16], the author mentions seven general factors which predetermine the features, and performance of the products, obtained via sol-gel route:

- Chemical composition of the liquid medium
- Chemical composition of the precursors (alkoxides)
- Molar factor (ratio between the alcohol, and the alkoxides)
- pH of the medium
- Presence of additives
- Temperature
- Pressure and chemical composition of the gaseous medium over the gelling system during the dry (annealing) process.

When more than one alkoxide is represented in the sol-gel system than the respective product could have more than one metallic element in its composition. This system is well illustrated in Figure 8:

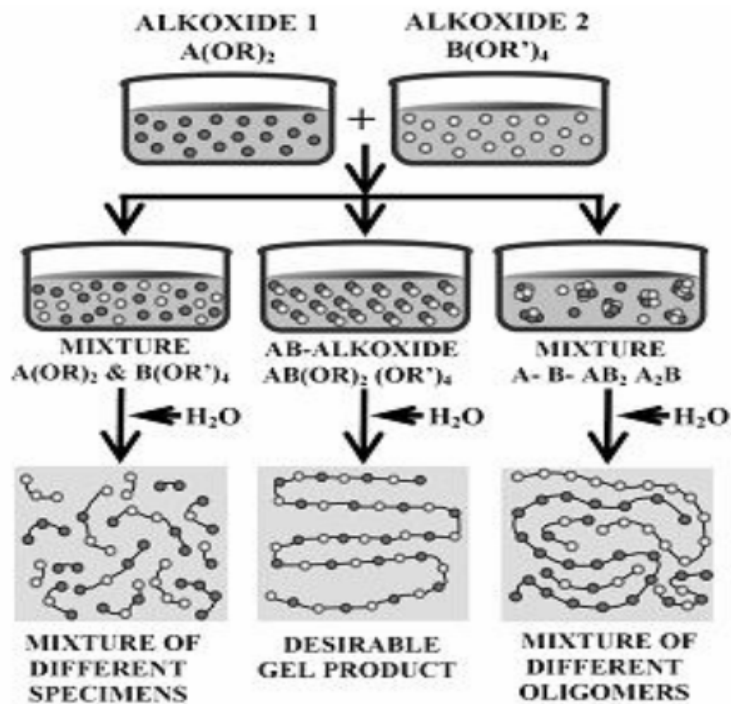


Figure 8. Sol-gel system with co-polymerization of two different metal alkoxides [16]

The correct performance of sol-gel process in case of two different metal alkoxides recommends information regarding hydrolysis aptitude of the respective alkoxides. The alkoxide with higher aptitude should be added to the system after the other.

1.4. Hybrid primer coatings – basic concepts and definitions

The hybrid materials belong to the newest generations of materials, object of research and development during the recent decades. The interest related to this group of materials originates from their ability to combine desirable properties (benefits) of both of organic and inorganic materials.

Karl Heinz Haas and Klaus Rose [22] have divided the solid materials into four basic groups, according to their basic matrix: 1- purely inorganic networks (glass and ceramics); 2- organically modified inorganic networks (silicones); 3- Organic crosslinking, inorganic organic networks (hybrid polymers); 4- purely organic polymers (plastics, resins, and etc.).

In that means, the benefits of the application of the hybrid materials as primer coatings have been emphasized by Zheludkevich [21]. He remarks that the hybrid primer coating combines the desirable properties of both of organic and inorganic moieties, and by that manner it forms reliable and durable barrier layer with remarkable corrosion protective ability.

Having in account the mentioned above benefits of the hybrid primer coatings, it could be concluded that they belong to the class of the *advanced materials*.

The following figure clearly represents the combination of properties, rendered by the hybrid primer coatings.

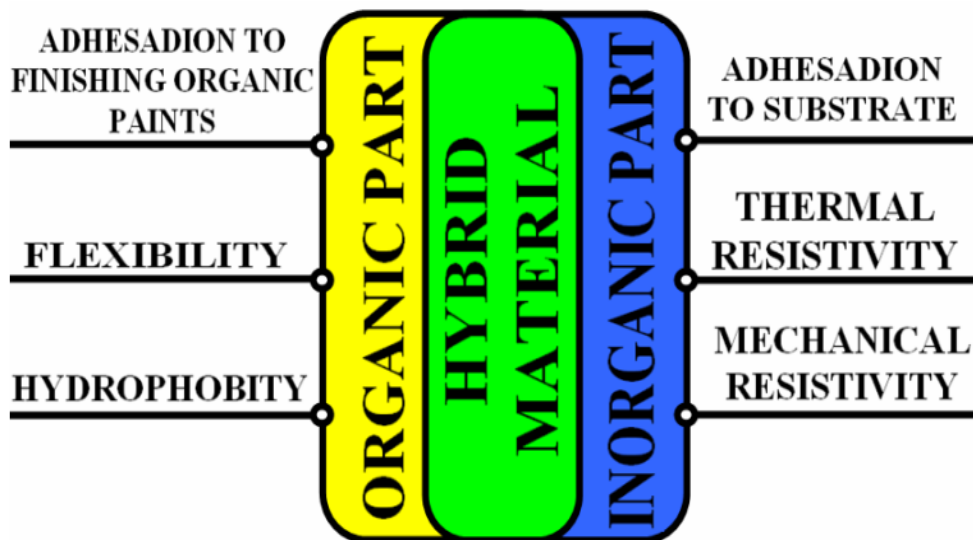


Figure 9. Combination of properties possessed by hybrid primer coatings

Further, in the same article, Zheludkevich represents schematic profile of hybrid primary coating (or sol-gel coating), which is shown below in the present text.

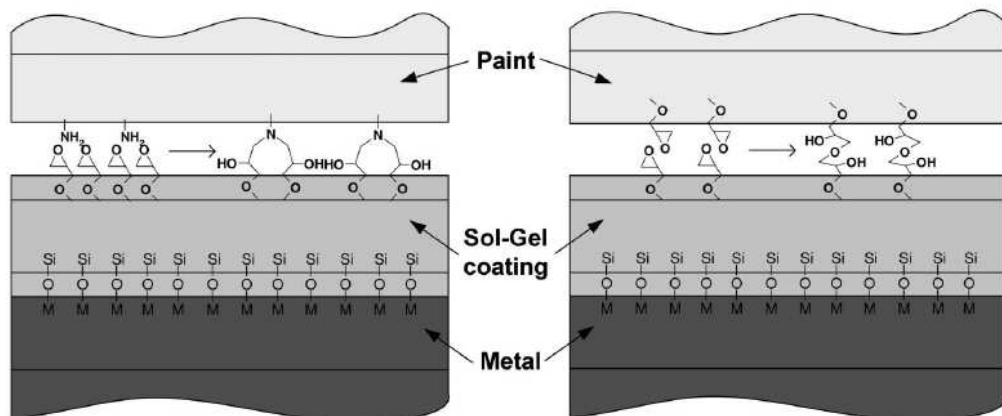


Figure 10. Schematic view of hybrid primer coating together with the layers above and below it, according to Zheludkevich [21].

Tsaneva et al. [13] described the completed coating systems, used in the conventional aircraft industry as multilayer, as it is shown in the Figure 11:

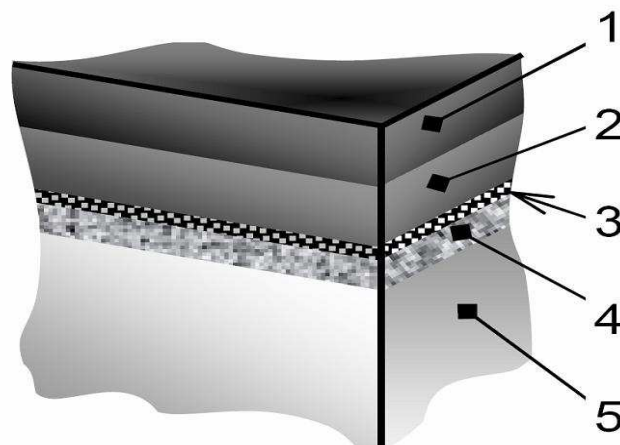


Figure 11. Schematic presentation of multilayer coating system according [13].

1,2 – finishing double layer of polyurethane, 3 – intermediate adhesive layer; 4 – primer hybrid coating; 5 – metal substrate

Despite the advantages described above in the present text, the hybrid materials should be further improved, in order to obtain more reliable durable protective coatings. In that means, Palavinel [25] has discovered that the hybrid materials reveal partial permeability for species originated from the corrosive medium. He has represented schematically a hybrid primer coating, with inclusions of penetrated water molecules, as well as various corrosive ions (Figure 12):

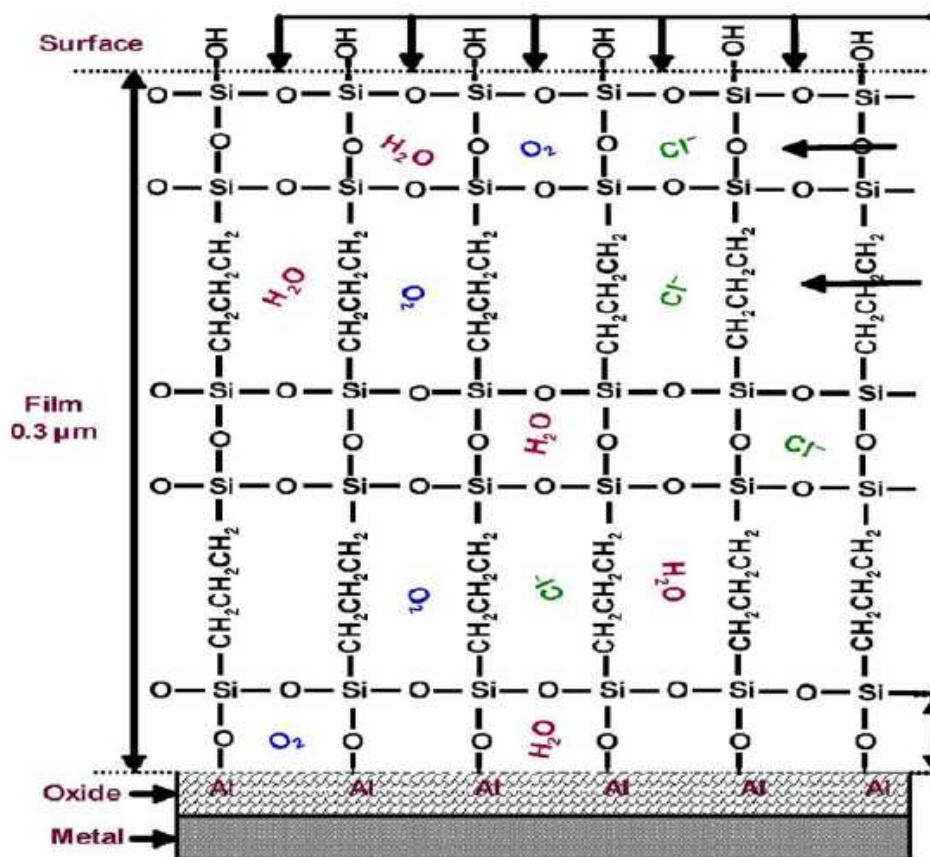


Figure 12. Schematic view of hybrid coating with inclusion of various corrosive species [26].

That disadvantage could be significantly diminished, by application of metal alkoxides with larger aliphatic chains. Frignani and coauthors have done [26] comparative assessment of primer coatings, obtained from alkoxides with different using aliphatic chains, as follows: *n*-propyl trimetoxisilane- $C_3H_7-Si-(OCH_3)_3$; *n*-octyl trimetoxisilane- $C_8H_{17}-Si-(OCH_3)_3$; *n*-octadecyl trimetoxisilane- $C_{18}H_{37}-Si-(OCH_3)_3$ and bis-trioximethyl-silil-ethane - $(CH_3O)_3-Si-C_2H_7-Si-(OCH_3)_3$. As conclusion, the authors have established that the larger aliphatic chains enhance the obtaining of thicker layers. These layers reveal aptitude for self assembling, and this kind of hybrid materials is also known as (SAM - selfassembled monolayers). They have significantly lower number and size of defects in their structures, and thus enable more efficient protection via formation of dense barrier layers [26, 27].

In addition, the SAM-layers reveal additive self-recuperation ability, due to the flexible character of the large aliphatic chains [28 - 30]. In addition, between the large aliphatic chains predetermine remarkably stronger Van der Waals's intermolecular interactions, occur. The latter, predetermine formation of self assembled dense barrier layers [32, 33] (Fig. 13).

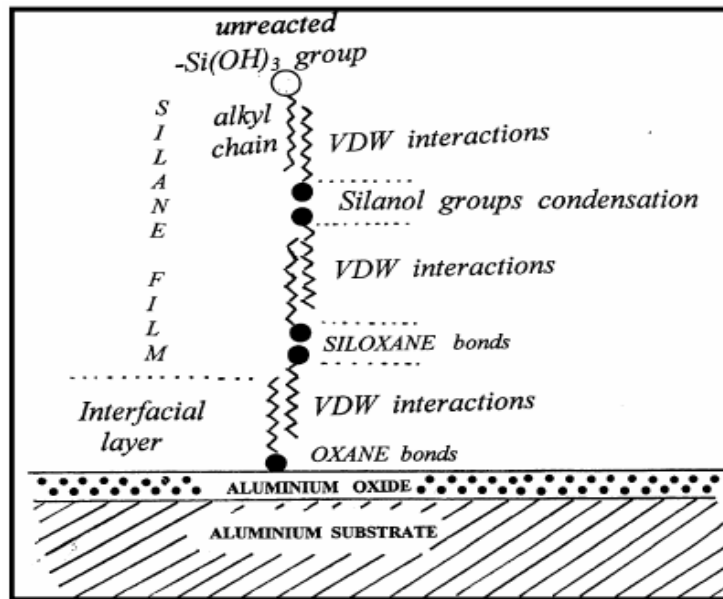


Figure 13. Schematic view of self assembled barrier protective film on aluminium surface [27].

Undoubted evidence for the reliability of the concepts described above in the present text is represented by the direct comparative observations performed via Scanning Electronic Microscopy (SEM), by Ono and co-authors [34].

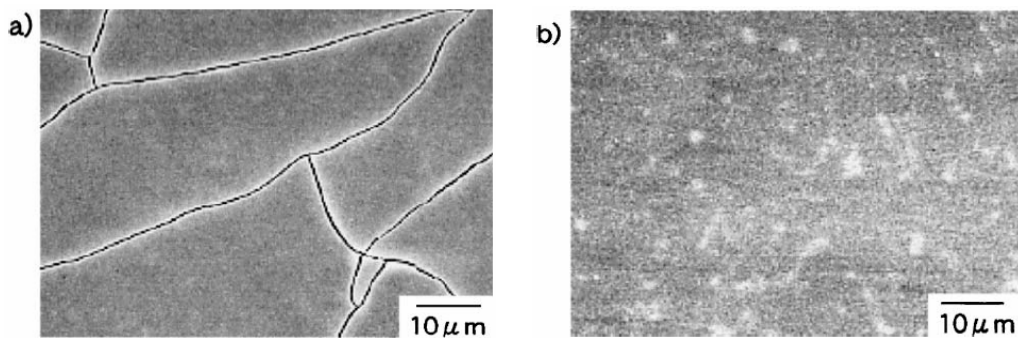


Figure 14. SEM images of silica and silica-polymer hybrid films
a – film composed by pure silica; b- film composed by silica + 0.5%wt. of poly (vinil-butiral) [35].

The authors [34] have undoubtedly evinced that the hybrid coatings superior the inorganic coatings, due to the flexibility of the hybrid matrix, originated from the organic moiety represented in its composition.

On other hand, the inorganic part of the hybrid material renders enhanced ability for adhesion to the metal substrate, by Van der Waals intermolecular interactions, which convert to covalent bonds between the natural oxide layer of the aluminium, and the partially hydrolyzed metal alkoxides, represented in the corresponding sol-gel system. Figure 15 shows schematic presentation of the transition of the Van der Waals intermolecular interactions to covalent bonds, during coating process of aluminium substrate by sol-gel system. Here, should be mentioned that, according to the literature [35], the native oxide layer is consisted generally by boehmite γ -AlO(OH), with thickness relatively equal to 5 nm. Thus, during the coating by sol-gel system, the alkoxides from the system interact with the oxide layer of the substrate, according to Zheludkevich [21].

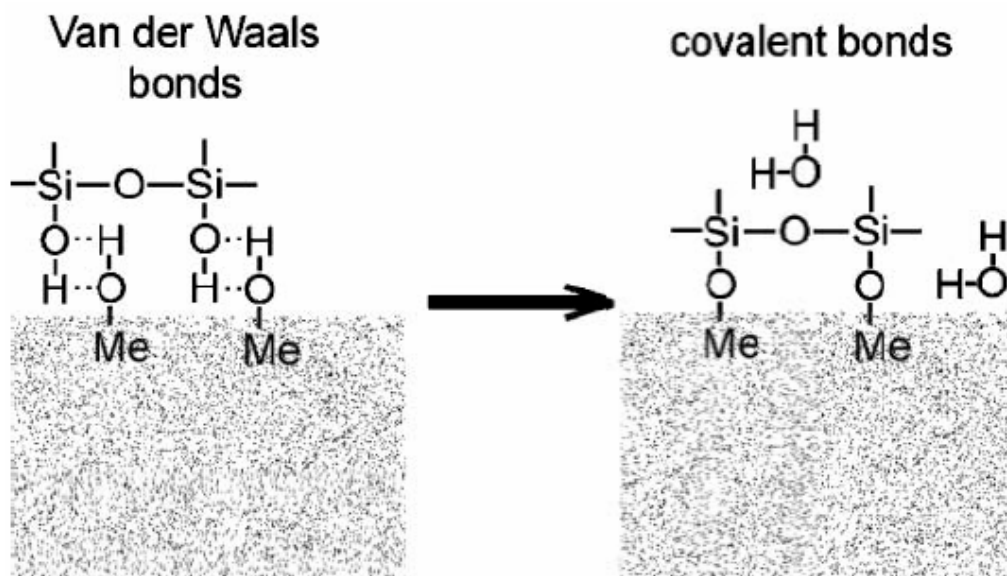


Figure 15. Schematic presentation of formation of covalent bond-connections between sol-gel derived primer coating and metal oxide layer [21].

1.5. Concepts for active and passive corrosion protection

The passive corrosion protection of the primer coatings towards aluminium alloys relays the formation of dense surface layers with absence of whatever defects (cracks, ruptures, deviations of the thickness etc.). In addition, the mentioned surface protective films should possess good adhesion to the metal oxide layer, in order to perform satisfying corrosion protection. On the other hand, the protective layers should reveal remarkable durability in labour conditions. Despite of the expressed durability given protective film, it always suffers deterioration of its properties due to ageing process. The deterioration could origin either from partial hydrolysis M-O-R bonds of the composing alkoxides, or damage from external source.

The properties of the protective films related to passive protection are already discussed in detail above in the present text (section 1.4).

The active corrosion protection should reveal after damage already represented in the structure of the protective coating. The basic approach to acquire active corrosion protective ability is by introduction of corrosion inhibitor into the composition of the protective layer. This class of substances (corrosion inhibitors) could be described as compounds which are able to hinder or retard the corrosion processes occurring in the zone of the defects represented in the structure of the protective layer. The mechanisms of their activity are described below in the present text.

1.6. Hybrid nano-composite primer coatings. Basic concepts

As it is mentioned above, the hybrid nano-composite coatings excel the hybrid coatings due to presence of reinforcing phase in form of equally distributed nano-particles in their structures [16, 17]. The presence of this reinforcing phase leads to increase of the thickness, as well as suppression of the aptitude of the primer coatings to form disruptions, during the annealing process. Here, should be mentioned that the diameter of the nano-particles should be less than 300 nm.

Further, the hybrid nano-composite primer coatings could be classified into three basic groups, regarding the interaction between the inorganic and the organic parts in the

hybrid matrix, as follows: 1- with absence of chemical bonds between them (a); 2- with presence of chemical bonds, between the inorganic and organic parts (b); 3- with presence of chemical bonds between the inorganic part and non-polymerizable organic moieties (c).

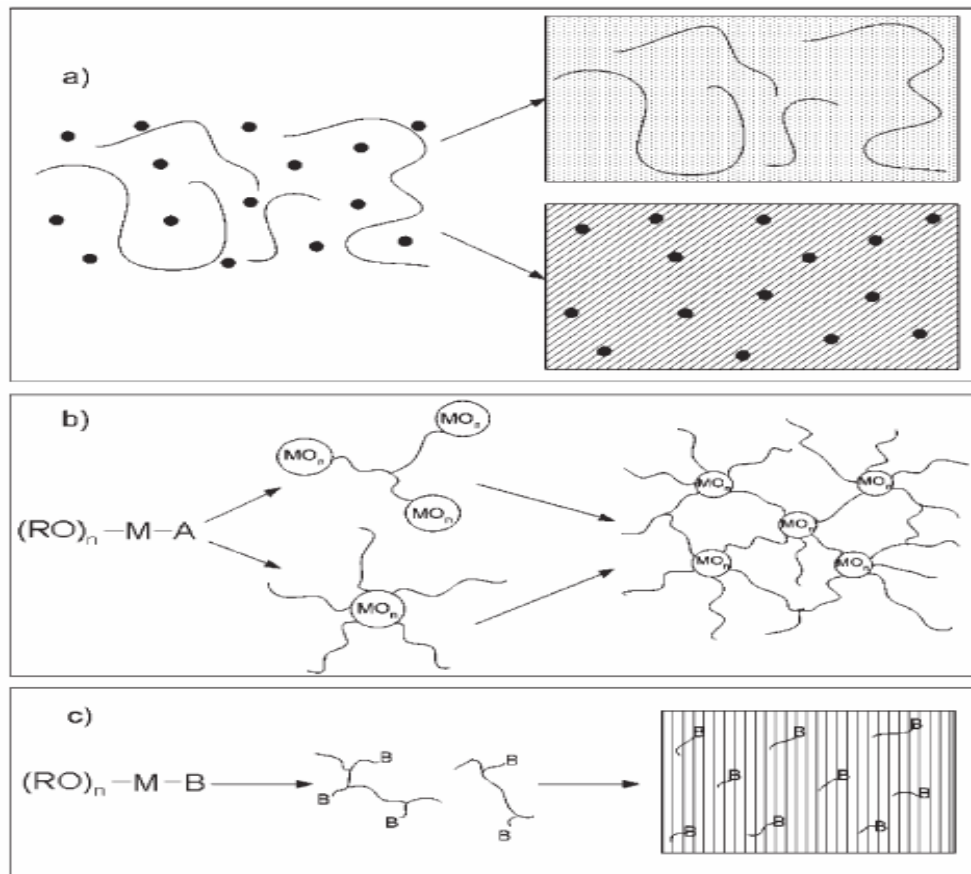


Figure 16. Various kinds of hybrid – nano-composite materials according to Zheludkevich [21]

In the literature, there is an example for obtaining of hybrid nano-composite primer coating, obtained by polymerization of hybrid matrix in colloidal liquid medium, with dispersed SiO_2 [31]. The author describe their product as hybrid nano-composite primer coating with significantly stable structure, where the OH^- groups are adsorbed on the surface of the silica particles, and they interact with the partially hydrolysed TEOS, resulting in formation of stable hybrid nano-composite systems.

The basic problem, related to the application of this kind of technologies is the agglomeration of the particles during the synthesis process. It could be avoided by addition of surfactants and detergents to the system.

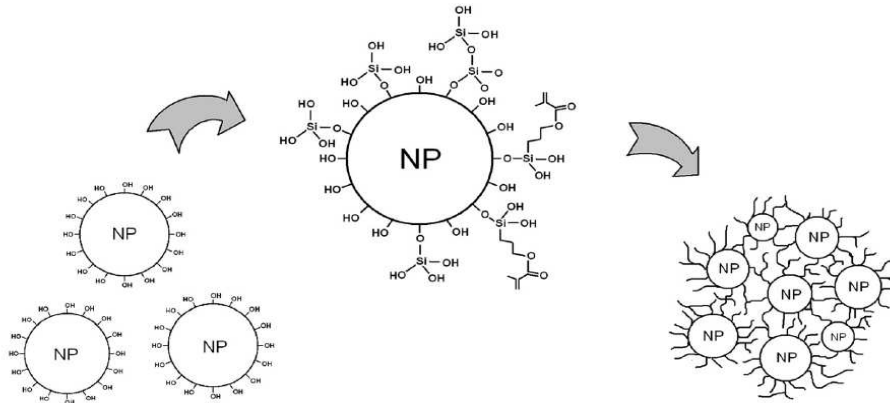


Figure 17. Schematic presentation of nanoparticles inclusions during hydrolysis-polymerization processes of the matrix [31].

Alternative approach for synthesis of hybrid, nano-composite primer coatings is via formation of nano-particles into the sol-gel system, during its synthesis. This process, of “in-situ”- synthesis of hybrid nano-composite primer coatings, is known as (Self-assembling of Nano-Particles - SNAP) [35 - 38].

If the nano-particles are previously impregnated by corrosion inhibitor, than the former serve as containers or reservoirs for the corrosion inhibitor. Thus, the nano-particles have a double role, as reinforcing phase for the hybrid matrix, and carriers of inhibitor, which supply its gradual release in the zones of the scratch, rupture or another defect of the primer coating, as is shown on figure below:

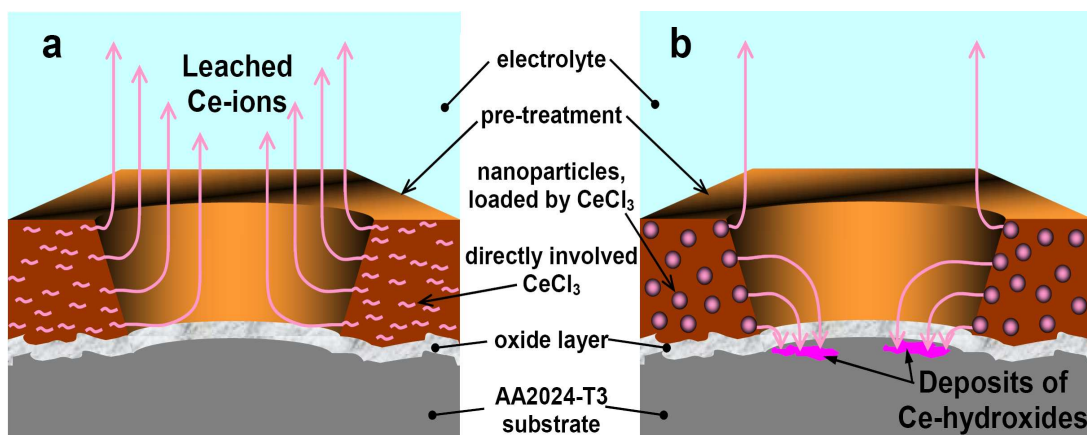


Figure 18. Schematic view of high (a), and low (b) rate of inhibitor leaching [39]

When inhibitor's gradual release occurs, than the undesirable process of its leaching could be suppressed, and thus, higher efficiency of its inhibitive effect could be expected. This concept is described adequately by Zheludkevich and co-authors [40].

During last decades, the chromium containing compounds were widely used as corrosion inhibitors, for various industrial applications. However, the chromium compounds have evinced as toxic and carcinogenic, and their use was limited by the European Community restrictions [41, 42] as it was mentioned above in section 1.3.1.

The mentioned directives initiated scientific efforts regarding investigations over environmentally friendly efficient alternatives of the chromium containing compounds. Among the available substitutions of the chromium compounds, the lanthanides have revealed the highest potential as corrosion inhibitors [43, 44]. In that means, Voevodin & co. [45] have investigated epoxy-zirconia primer coatings with inclusions of $Ce(NO_3)_3$, $NaVO_3$, and $NaMoO_4$ inhibitors. As result the authors have established that the first one possess the best inhibitor's ability. As confirmation of this conclusion, Hamdy and Beccaria [46] have also found that the cerium compounds reveal the best behaviour among the lanthanides. Further, they have established that the best inhibitive effect belongs to $CeCl_3$, and in addition, it even is comparable to the chromates' protection effect, respectively..

1.7. Mechanism of the inhibitive effect of the lanthanide's compounds on the corrosion processes

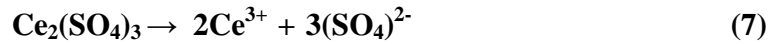
Here, should be mentioned that the essential nature of the of the inhibitive effect of the compounds of lanthanide elements could be described as formation of secondary, derivative barrier film, formed by precipitation of products of chemical interaction between the Ce – compound and species from the corrosive medium.

By other words, the inhibitor's effect of the Ce-salts is consisted on formation of derivative secondary barrier insoluble layer composed by Ce-oxides, and hydroxides as a product of chemical reactions between Ce^{3+} or Ce^{4+} cations, originated from the dissolved Ce-salt in the electrolyte, and OH^- ions. The hydroxyl ions are product of the cathodic

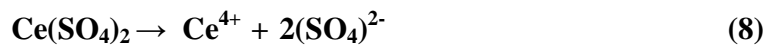
partial reaction of the corrosion (see reaction 1, and Figure 3). Yasakau et. at. [43] described this mechanism in details.

Chemically, the conversion of the soluble Ce-salt to insoluble barrier protective layer of sediments could be described as follows:

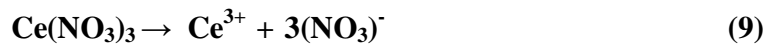
- Dissolution of the corresponding Ce-salt by dissociation, for example:



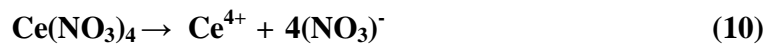
dissociation of Ce(III)-sulphate into the composing ions



dissociation of Ce(IV)-sulphate into the composing ions



dissociation of Ce(III)-nitrate into the composing ions



dissociation of Ce(IV)-nitrate into the composing ions

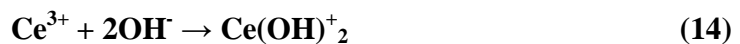
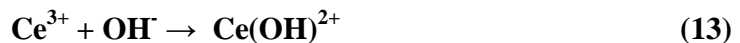


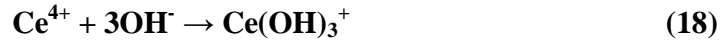
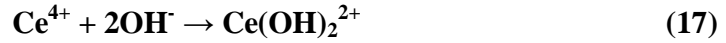
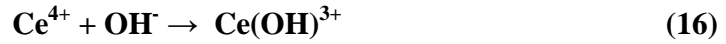
dissociation of Ce(III)-chloride into the composing ions



dissociation of Ce(IV)-chloride into the composing ions

These processes are followed by chemical reactions of interaction of the Ce-ions, as product of the above described reactions (7-9), and OH⁻ anions, from the cathodic partial reaction of the corrosion (see eq. 1). The products could possess a form of either complex ions in the solution, or insoluble sediments, as is shown by equations 13 – 19:





Here, should be mentioned that according to the authors [43, 47], the complex ions also could convert to insoluble sediments depending on the pH value of the environmental medium (not shown in the Figures). In addition, they suggest, that the derivative Ce-sediments could possess a composition, which could be described as hydrated cerium oxide $\text{CeO}_2 \cdot 2\text{H}_2\text{O}$. This concept is discussed by Aldykiewicz and Davenport [48], as well.

It is necessary to underline, that the influence of the compounds of the lanthanide elements looks to be rather contradictive. While some authors describe an additive beneficial effect of the involved, Ce^{4+} -ions over the polymerization, during the preparation of the coating [49], other authors observe a negative effect over the barrier properties of the respective coatings [47]. The former concept is generally based on the idea, that the Ce-ions form coordination bridges with polymer chains of the hybrid primer coating, as it was described by Kozhukharov [16] as well. That additive process should lead to a beneficial additive densification of the obtained barrier film. The latter concept describes the opposite phenomenon of decrease of density.

This phenomenon is consequence of dissolving of the enclosed in the bulk of the coating layer inhibitors salts are in the form of solid crystals. When the coating layer is in contact with electrolyte, the corresponding crystals dissolve, by other words it transits to the liquid phase of the medium (see reactions 7-12). As result, the space occupied by the solid crystals of the lanthanide salt undergoes electrolyte invasion. Thus, due dissolving of the inhibitor's salt, a cavities, filled by electrolyte are formed. Furthermore, these cavities transform to a pathways of electrolyte penetration. Consequently, the electrolyte reaches the metal surface much easily, because these pathways facilitate its access.

Logically, it leads to deterioration of the barrier ability of the coatings. After the conversion of the coating layers from dense films into hollow structures, filled by electrolyte, they could not serve as efficient dense barrier between the metal surface and the corrosive liquids, (such as NaCl solutions in water). This effect is observed at direct addition of various inhibitors as: $\text{Na}_2\text{Cr}_2\text{O}_7$, $\text{Ce}(\text{NO}_3)_3$, Na_2MoO_4 and NaVO_3 during preparation of glycidooxypropyl-trimethoxysilane [37]. As result, the authors report that they have observed various levels of negative impact on the barrier properties of the corresponding hybrid coating (composed by glycidooxypropyl-trimethoxysilane). Finally, they conclude that among the inhibitors used, the highest negative impact belongs to Na_2MoO_4 and NaVO_3 .

Hence, this negative effect should be avoided via encapsulation of the corresponding inhibitors into carriers. This effect could be achieved via application of different technologic approaches.

1.8. Technologic features of the production of hybrid nano-composite primer coatings

As it was mentioned above in the present text, and even illustrated in Figure 8, position b, the inhibitor could be involved into nano-particles, prior its addition to the sol-gel system, during the synthesis of the respective hybrid primer coating. Hence, the nano-particles have a double role, as reinforcing phase for the hybrid matrix, as well as carriers of corrosion inhibitor.

Namely, the technology for the preparation of the corresponding hybrid nano-composite primer coatings includes two intermediate stages:

(i)- Obtaining of colloidal system, composed by solid phase represented by the nano-particles, dispersed into a liquid medium consisted on solution of the inhibitor's lanthanide salt into liquid solvent.

(ii)- Gradual saturation of the obtained colloid by evaporation of the liquid solvent, in conditions of intensive perturbation in order to obtain a slurry system. For some cases,

supplementary addition of detergents could be necessary, in order to suppress undesirable agglomeration of the nano-particles.

Optional is a drying procedure, in order to obtain dry powder material composed by hollow nano-particle's agglomerates incorporated by corrosion inhibitive substance. Finishing ball milling could be applied, in order to diminish the size of the derivative clusters.

After all these procedures, the obtained slurry, or powder (composed by anano-particles, with impregnated inhibitor in) could be applied into the corresponding sol-gel system. The obtained conjugate is deposits over the metal substrate. After the accomplishment of the hydolysis-polimerization processes the obtained polymer hybrid matrix encloses the clusters of nano-particles together with the involved inhibitor inside.

Examples for synthesis of hybrid nano-composite primer coatings could be found in the literature [4, 7, 12, 13], and also was object of innovation patent issue [50].

1.9. Alternatives for the self healing coatings containing inhibitors

Stephenson and Kumar propose alternative approach for obtaining of coating materials, with self-healing effect [51]. The principle of self-healing effect in their case is rather different. They enclose microcapsules in the organic polymer matrix. In their case, the microcapsules used do not contain any polymerized media. When the integrity of the microcapsules is corrupted, due to mechanical scratch, the internal liquid content goes to the surface, filling the zone of the scratch. Afterwards, it polymerize vs. the time due to interaction with the air, because its exposure to the environment.

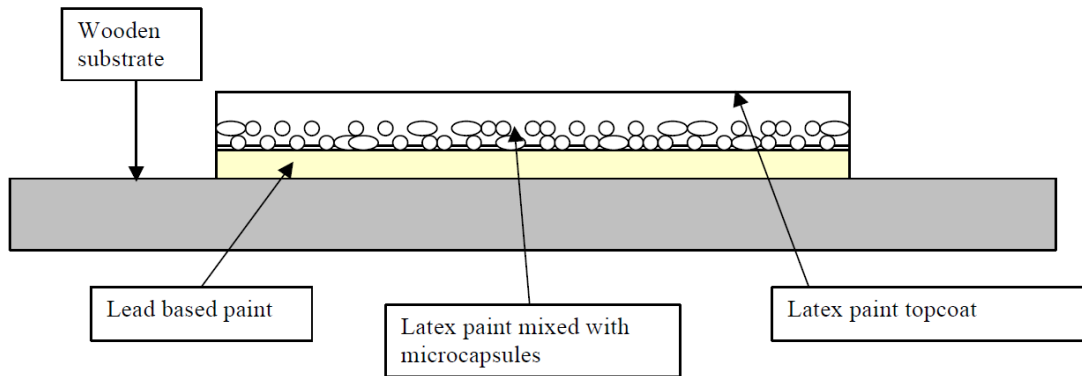


Figure 19. Schematic presentation of coating on wood with included microspheres [51]

This approach is achieved by incorporation of urea-formaldehyde microspheres into the composition of organic coating. For demonstration of this approach, the authors made actual contrast photography of the coatings, as is shown in Figures 20 and 21:

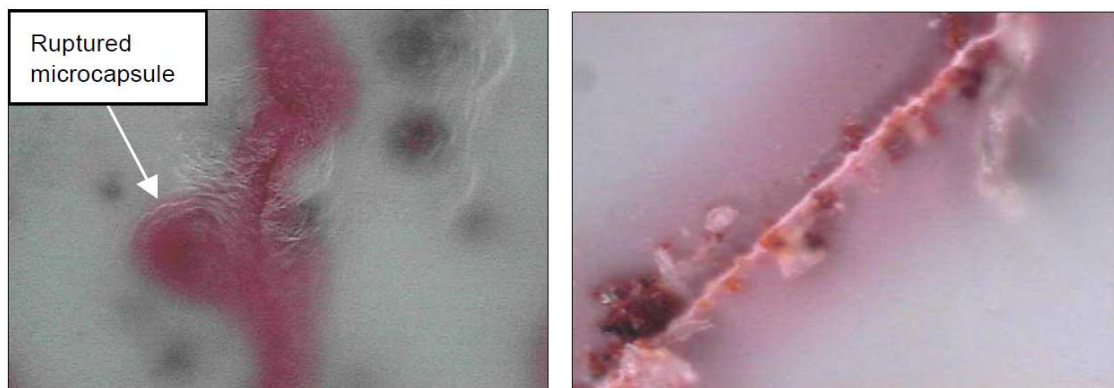


Figure 20. Photographic images of coatings with inclusions of microspheres with colorant after artificial defect [51]

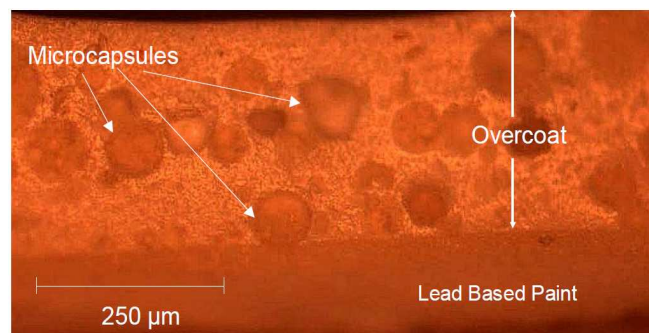


Figure 21. Images obtained via refractive optical microscopy of cross-section of coating with included microspheres [51]

Liu and co-authors [52] have investigated the process of involvement of microspheres of polystyrene in hybrid matrix composed by poly-tetrabutyl ortotitanate $n[(C_4H_9O)_4Ti]$. Afterwards they have dip-coated glass substrates. The deeping process of the coating on the glass substrate is shown in Figure 22 (a). Figure 23 shows Scanning Electronic Microscopy photographs of polystyrene microspheres surface agglomeration.

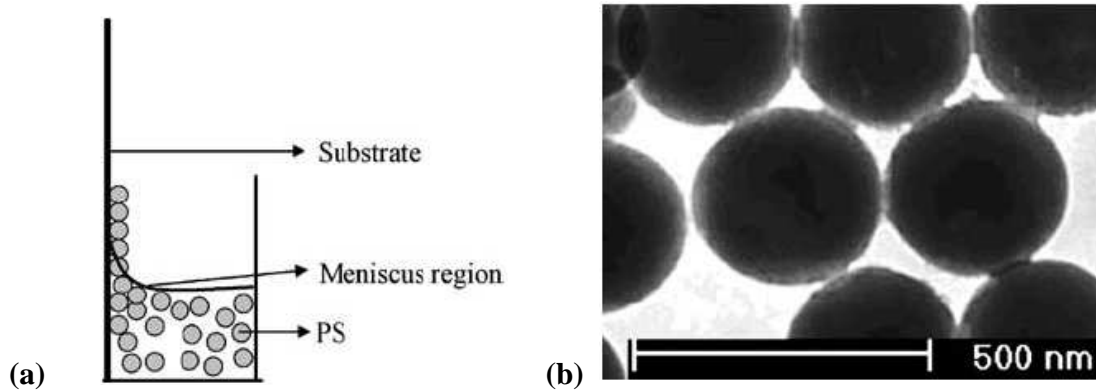


Figure 22. Schematic presentation of dip-coating procedure of deposition of coating with microspheres (a); Image of microsphere obtained by means of Transmission Electronic Microscopy (b) [52]

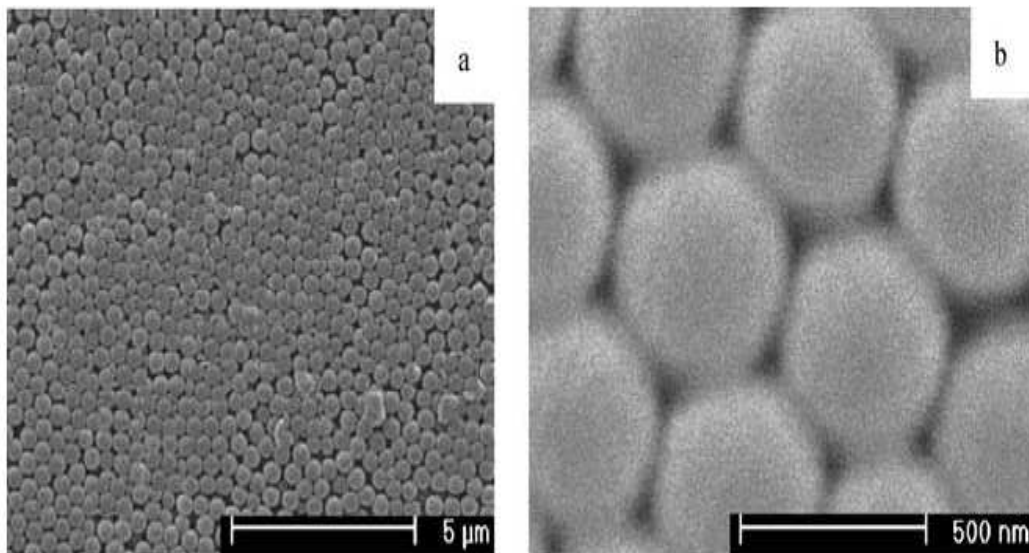


Figure 23. SEM photograph of polystyrol microspheres at different magnifications [52]

1.10. Basic concepts and definitions related to the Electrochemical Impedance Spectroscopy

1.10.1. Basic elements of the impedance

Each passive AC electric chain (“passive chain”- means electric chain which doesn’t contain internal source of electric energy) could be composed by three basic groups of elements, connected in series or/and in parallel among them. These groups are as follows: *active resistance* “**R**”, *capacitor* “**C**” and *inductance* “**L**”. When AC-electric tension, is applied, every one group of elements reveal different (individual) resistance against the respective electric current.

a). Resistance of electric chain with active resistance: This kind of resistance is frequency-independent. It value could be calculated via the following equation:

$$R = U / I = U(t) / i(t) = U_{\max} \cdot \sin(\omega \cdot t) / I_{\max} \cdot \sin(\omega \cdot t) = U_{\max} / I_{\max} \quad (20)$$

where: U – is the DC- tension (V); I – DC- current (A); $U(t)$ – AC- tension; $i(t)$ – AC- current; U_{\max} – amplitude of the AC- tension; I_{\max} – amplitude of the AC- current; ω – angular (radial) frequency rad./s

For electric chains composed only by this kind of resistance, it doesn’t depend on the frequency. The sinusoidal curve dependences of the current from the time overlap – of the potential (tension), as is represented in the Figure 24.

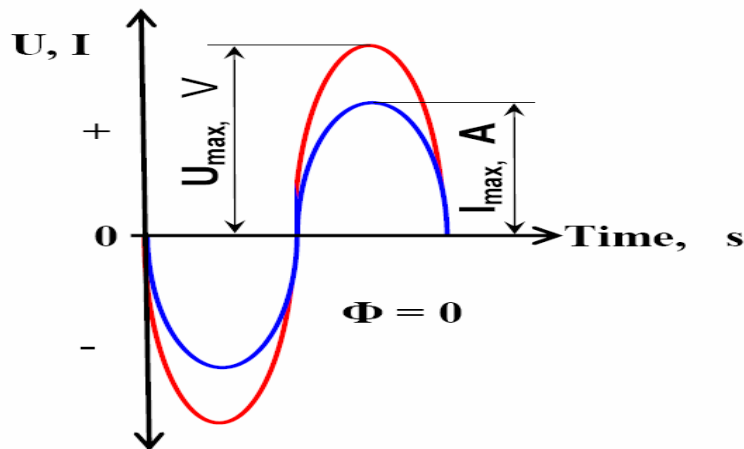


Figure 24. Sinusoidal curves of the current and potential within the time.

b). Resistance of electric chain, composed only by capacitive element: When direct tension is applied to chain with capacitive element, its resistance inclines towards endlessness (infinity), consequently through this chain could not pass any measurable (detectable) currents. However, when alternating tension is applied to the chain, the plates of the capacitor begin to charge/discharge periodically and consequently an alternating current commences pass through the chain. In that case, phase shift (φ), between the sinusoids of the current and the tension appears. The current's sinusoid shifts before this of the tension with angle equal to 90° ($\pi / 2$), as is depicted below:

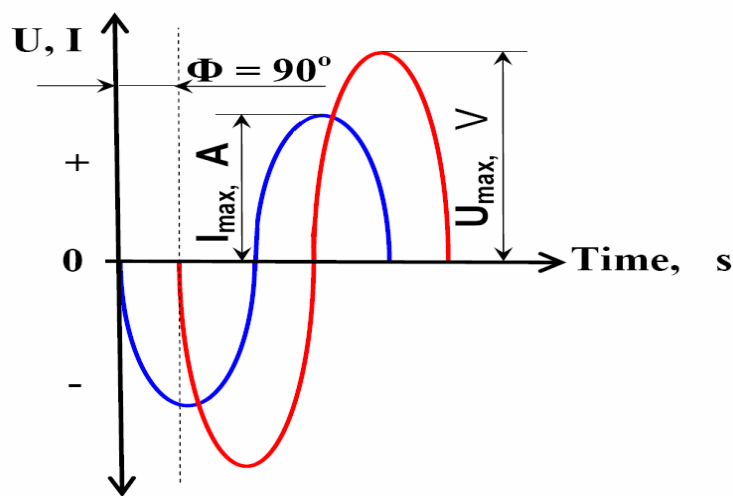


Figure 25. Sinusoidal curves of the current and potential within the time.

The capacitive resistance X_C of AC- chain with capacitor is in dependence of the frequency – ω , and the capacity C of the capacitor, according to the following expression:

$$X_C = 1 / \omega C \quad (21)$$

Where: X_C – capacitive resistance; C – capacitance (F)

The capacitive resistance X_C differs from the active Ohmic resistance, because the former depends on the frequency. It is also known as “reactive” resistance.

c). Resistance of electric chain, composed on inductance: When direct tension is applied to chain with inductive element, its resistance neglectable, and high current passes through it. When alternating tension is applied to the chain, through the windings

(coils) of the inductor passes a current, which induces derivative currents in the opposite direction. In that case, phase shift (ϕ), between the sinusoids of the current and the tension appears. The current's sinusoid shifts after this of the tension with angle equal to -90° ; $-(\pi / 2)$, as is shown in the Figure 26:

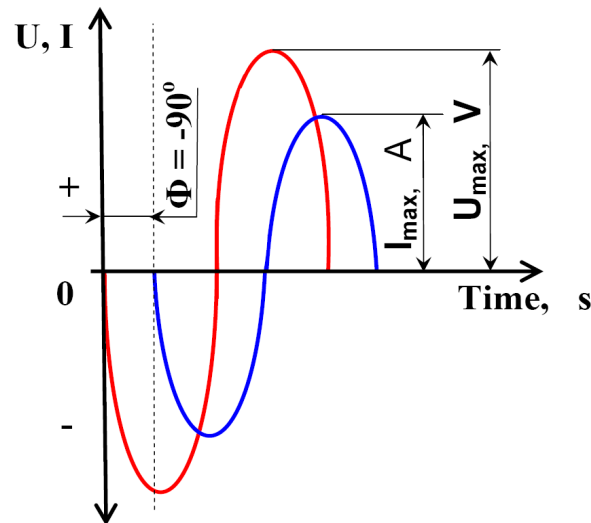


Figure 26. Sinusoidal curves of the current and potential within the time.

The inductive resistance depends on the frequency according to the following formulae:

$$X_L = 2\pi fL \quad (22)$$

Where: X_L is the inductive resistance; L – inductance (H).

The inductive resistance increases proportionally to the frequency of the applied tension.

Impedance (Z) – It is the total resistance of AC chain composed by various kinds of resistance, connected by different manners.

Because its quantitative determination is extremely difficult task, it is preferable to express it in form of complex number z , consisted of both real a and imaginary jb parts:

$$z = a \pm jb \quad (23)$$

The real part is ascribed to the active (Ohmic) resistance (R), while the imaginary part is related to the reactive resistances (C and L).

$$Z(\omega) = R + X_c = R + (1 / j \omega c) = R - j(1 / \omega c) = Z_{Re} - Z_{im} = Z' - Z'' \quad (24)$$

The equation 24 reveals the dependence of the impedance from the applied frequency. The multitude of values of the impedance for different frequencies forms impedance spectrum.

1.10.2. Graphical presentation of the impedance spectrum:

It could be concluded that the value of the impedance depends simultaneously on the resistance, inductance, capacitance and the angular frequency, respectively.

Consequently it is possible to create a 3-D coordinate system, composed by R, C, and ω (and L, as negative values of C). In practice, two basic coordinate systems are accepted: (i)- Nyquist plot, where the imaginary compound $-Z''$ is depicted against the real Z' - value for each frequency, and (ii) - Bode plot, where both of the modulus of the impedance $|Z|$ and the phase shift ϕ are plotted against the linear frequency.

Figure 27 shows the impedance spectra for the individual R and C elements as well as their connections in series and parallel:

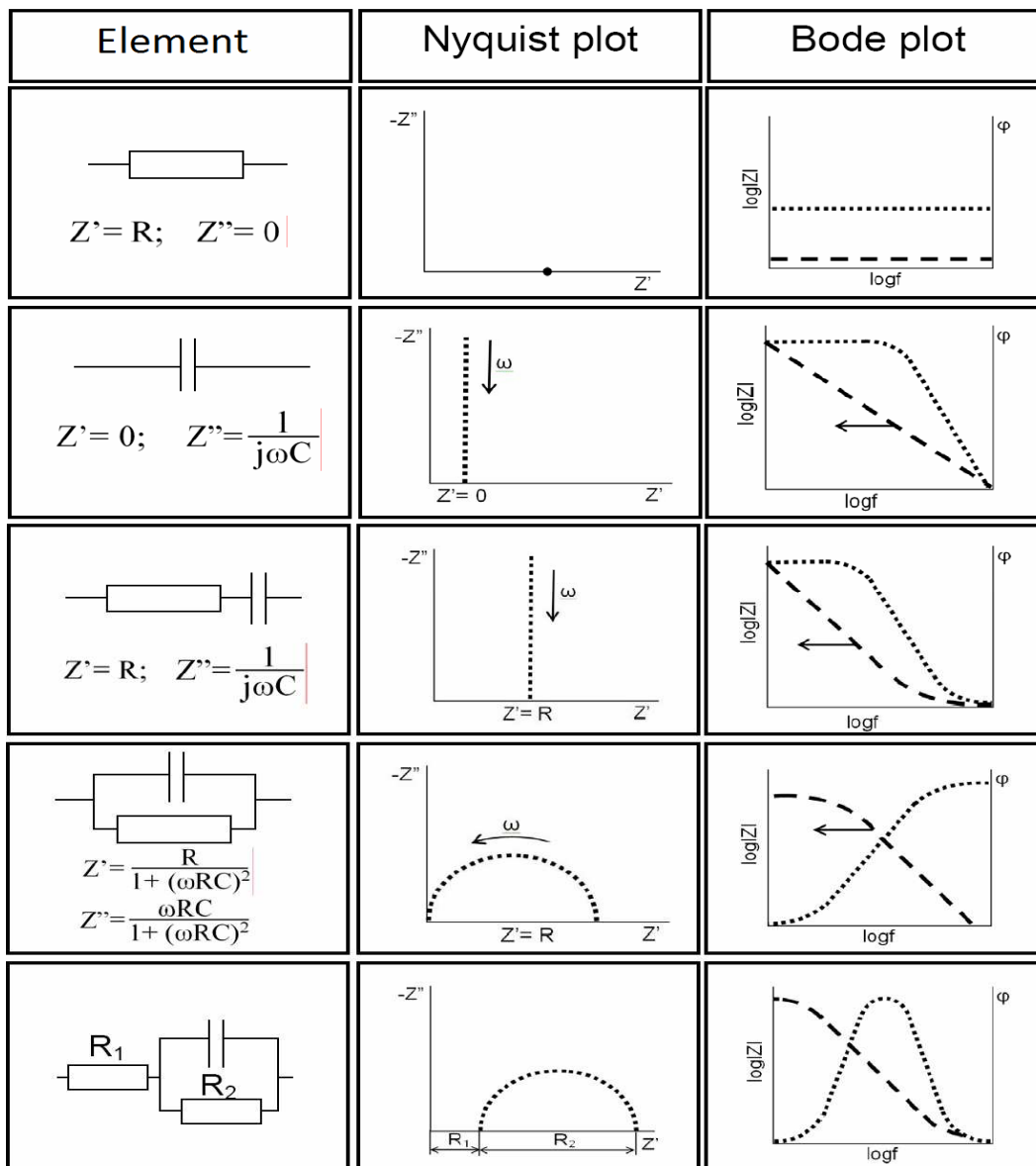


Figure 27. Basic examples for impedance spectra of various combinations between R and C.

1.11. Electrochemical impedance and impedance modeling

When AC- potential with relatively low amplitude (in order of 5 to 10 mV) is applied to electrochemical cell, the answer of the cell possess features of AC- chain, composed by active and reactive resistances, which form the total impedance, well known as *electrochemical impedance spectroscopy* (EIS).

Here, should be mentioned that despite the similarities between the impedance answers of given AC- electric chain, and given electrochemical cell, the nature of the processes of the latter (the cell) possess rather different nature. This difference originates from the fact that in the electrotechnical systems (the chains), the charge carriers are simply electrons, while in the electrochemical systems (the cells) the charge carriers are ions. The latter, suffer electrochemical and even chemical oxidation/reduction processes, diffusion, and ect.

The electrochemical impedance modeling for an electrochemical system is based on creation of an imaginable electric circuit, known as *equivalent circuit*. Here, the impedance is similar to the impedance response of the respective electrochemical cell.

In this context, the active and reactive resistances of the corresponding electrochemical cells could be ascribed to the following processes:

Active resistance: It is always ascribed to transfer of charge carriers (ions) in homogeneous field. The last one is characterized with absence of interphases. However, it also finds application for description of charge-transfer across interphase (electrode / electrolyte). In that case, the resistance describes all of the electrochemical reactions done, between species from the liquid medium and the metal piece, exposed to it (see equations 1 – 3, and Figure 3). Usually, this kind of active resistance is signed as R_{ct} , or “charge transfer resistance”. Alternatively, some authors prefer to use the term “polarization resistance” R_p .

Capacitive resistance: In the case of equivalent circuits always capacitive elements are added, when in the real electrochemical cells there are interphases (for example: solid/liquid; liquid/solid, or even liquid / liquid, such as water/oil). In all these cases, electric double layer occurs on the metal surface border (exactly the interphase between the solid and the liquid phases).

From physical point of view, the electric double layer could be described as potential barrier, composed by charge accumulation of two layers, which stay in defined distance between them. This model is well known as a model of Helmholtz & Peren [53]. In addition, the capacitance character could be owned by surface dielectric films on the metal surface, such as the native oxide layer on the aluminum surface.

In the equivalent circuits, each interphase could be described as parallel connection between resistance (R), and capacitance (C). Again, in short – the resistance relates to charge transfer between the metal, and species from the liquid medium, and the capacitance corresponds to the electric double layer. The **RC** parallel connections are also known as *time constants*. As it could be summarized from Figure 27, each time constant reveals as individual pick in the Bode plots, as well as individual semi-circle in the respective Nyquist plots. For highest point of the semi-circle, in the latter (Nyquist) plots relates to the following dependence:

$$RC\omega = 1 \quad (25)$$

The mathematician product $\tau = RC$ has units of (s), and consequently it is accepted as *time constant*.

Warburg Impedance elements: Again, the electrochemical processes possess much sophisticated nature, in comparison to these in the electric circuits. Hence, in addition to the relation of electrochemical processes to charge transfer (R), and charge accumulation (C), in the electrochemical systems occurs of diffusion of charge carriers (charged particles). The Warburg and the rest electrochemical impedance elements have not equivalents in the electronics, or electrotechnique. In order to model the diffusion processes, in 1958 Graham [54] introduces the element Z_w , (Warburg impedance). According to the laws of Fick for diffusion the Warburg impedance has the following expression:

$$Z_w = \frac{\sigma}{\sqrt{\omega}} (1-j) = \frac{\sigma}{\sqrt{\omega}} - j \frac{\sigma}{\sqrt{\omega}} \quad (26)$$

Where: σ – is Warburg's constant, ω – angular frequency; j – imaginary unit.

When very high frequencies are applied to an electrochemical cell as a result it makes the ions to vibrate around their positions. They vibrate following the oscillations of the electric field, and values of $\omega \rightarrow \infty$ and $Z_w \rightarrow 0$, are respectively.

However, at enough low frequencies values, the ions begin to perform “forward-backward” movements, which length corresponds to the amplitude.

The equation 26 reveals that the values of both the real and the imaginary parts of Warburg impedance are equal. Due to that reason, in the complex plane of the Nyquist plots the Warburg impedance appears in form of straight line with slope equal to 45°.

Here, should be mentioned that in ref. [55] different elements for expression of diffusion are also available. Their use is preferable, when the straight line has different slope, than 45°. Figure 28 represents the various kinds of diffusion expressing elements:

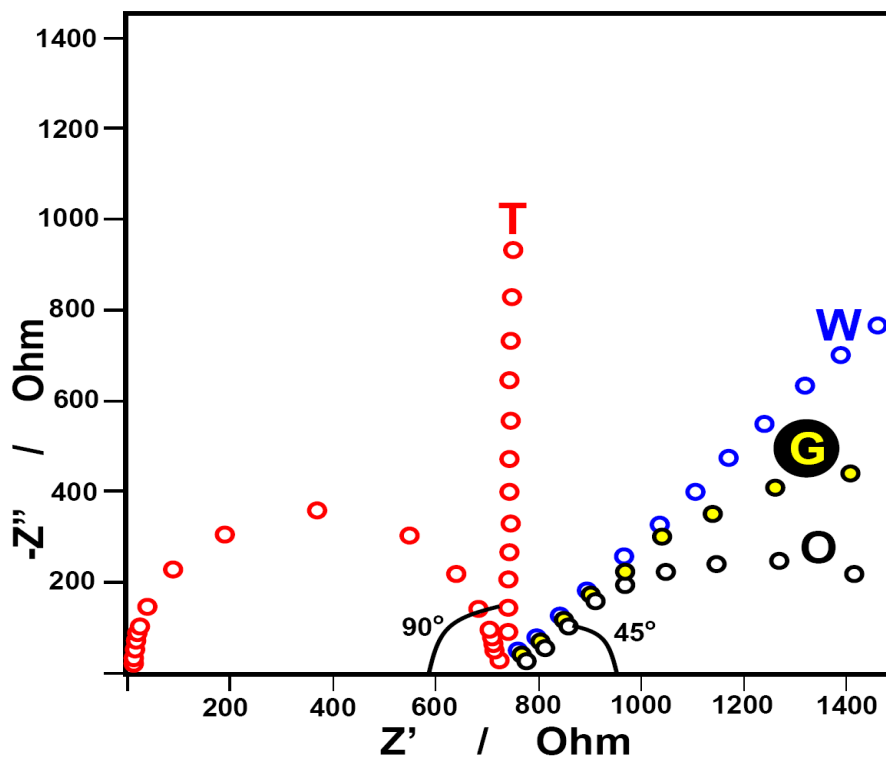


Figure 28. Nyquist plot, with different elements of diffusion illustration

T – Hyperbolic tangent element; W – Element of Warburg impedance; G – Element of Gerisher's impedance; O – Hyperbolic cotangent element

Constant Phase Element. In the case of the former, the phase shift φ could occupy different values than 90° ($\pi/2$ – typical for the capacitors). In that case in the corresponding equivalent circuit new element is involved. Its name is constant phase element (CPE), which phase shift is lower than 90°.

$$Z_{CPE} = \frac{1}{Y_0(j\omega)^n} \quad (27)$$

where: Y_0 is a constant and n is exponential multiplier.

This element possess rather character of formal approximation, because its physical nature is not enough clear. According to some authors, CPE could be ascribed either to the non-ideality of the surfaces (expressed by both of their roughnesses, and chemical compositions), or to the electric permeability of the bulks of the phases.

Certain physical significance could be ascribed to the constant Y_0 , only at defined values of n : $n = 0$; $n = 0,5$ and $n = 1$. These three particular cases are shown in Table 2.

Table 2. Physical significance of the constant Y_0 for the respective values of n

n	Equivalent	Physical significance	Measure according SI
0	Resistance	R^{-1}	$\Omega^{-1} = S$
0,5	Warburg element	σ	$\Omega^{-1} s^{0,5}$
1	Capacitance	C	$F = \Omega^{-1} s$

The most typical example for equivalent circuit for modeling of an electrochemical system of corrosion of metal in liquid medium is the “cell of Randles” [56] as is shown in Figure 29.

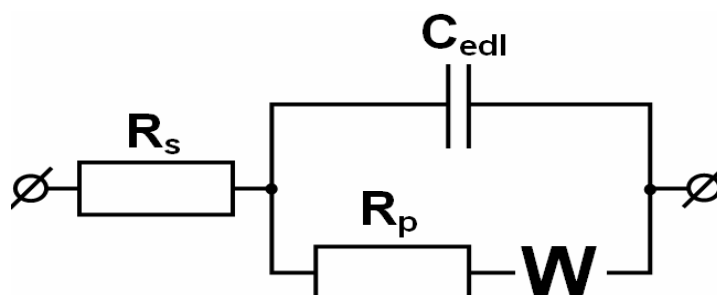


Figure 29. Structural impedance model for quantitative description of the electrochemical reactions, involved into the system: corroding metal / electrolyte [61].

In Figure 29 is presented the basic structural model of Randles, which describes rusting metal piece exposed to a liquid medium. The corresponding equivalent circuit is composed by four elements, which form one time constant, with included Warburg element, connected to additive resistance. Their signatures have the following meaning:

- R_s - Resistance of the solution. It also could be accepted as electrolyte's resistance by electrochemical point of view. Its value generally depends on the kind of the corresponding ions, as well as their concentration.

- R_p - Polarization resistance, known also as charge transfer resistance. It refers all of the electrochemical oxidation/reduction reactions (or by other words: anodic and cathodic partial reactions), composing the entire corrosion process.

- C_{edl} - Double electric layer's capacitance. It is related to the capacitance which appears always on the interface between the metal surface and the liquid medium (the electrolyte). Usually this element is substituted by CPE, in order to describe more precisely the features of the real electrochemical system.

- W - Warburg element - reveals all of diffusion, as well as adsorption/desorption processes which involve all of the species (ions), represented in the system.

1.12. Practice in the electrochemical impedance spectroscopy

The EIS could be accomplished by devices, named "Impedance spectrometers". They are usually connected to three-electrode cells, where the electrodes are simultaneously immersed into the electrolyte. The Working electrode (WE) is represented by defined surface of the investigated sample. The Reference electrode (RE) serves as observation point for the measurements. The Counter electrode (CE) serves as application. Thus, between the cell and the spectrometer there are two signal-transmitting electric chains: 1- Chain for output signals of the impedance response of the cell. This chain is enclosed between the Working electrode (WE) and the Reference electrode (RE) and 2 - Chain for input signals to the cell. It is enclosed between the working electrode (WE), and the Counter electrode (CE). Figure 30 shows the electrodes arrangement and control.

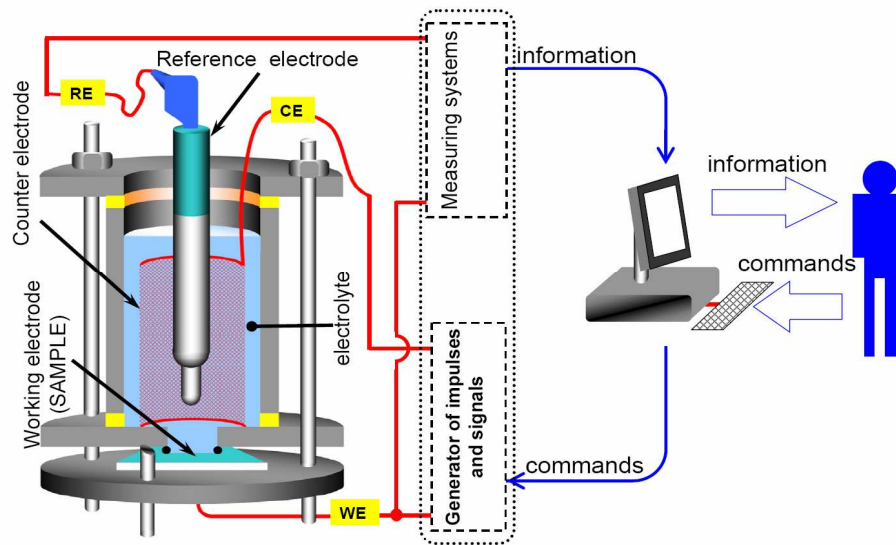


Figure 30. Principal scheme of equipment for electrochemical measurements

1.13. Topographic observations and description of the surface

The Atomic Force Microscope (AFM) is equipment for surface topographic observation. The unit consists of a microscale cantilever with a sharp tip (probe) at its end that is used to scan the specimen surface. The cantilever is typically silicon or silicon nitride with a tip radius of curvature in order of nanometers. When the tip is brought into proximity of a sample surface, forces between the tip and the sample lead to a deflection of the cantilever according to Hooke's law. This scanning is based on mechanical touch between a needle and defined point of the surface. By itself the needle is connected with a reflector element (mirror). From the top-side of the mirror, there are LASER-source (emitter) and LASER-receiver (sensor). Figure 31 shows a schematic view of the AFM – head unit used in the present study.

The settings parameters are respectively:

- **Setting Parameters:**

- Area for scanning (nm)²
- Scanning rate (speed)
- Resolution (number of data points) per one line

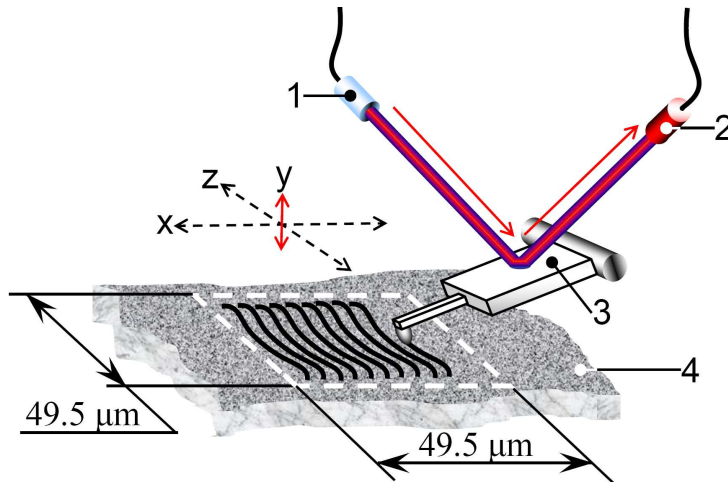


Figure 31. Schematic view of the atomic force microscope

1 – Laser emitter; 2 – light sensor; 3 – cantilever; 4 – sample's surface

• **Scanning Modes in 2D- (Figure 32) and 3D (Figure 33)**

- Static Mode: Direct moving of the needle on the surface
- Dynamic Mode: Based on vibration of the needle over the surface

• **Data Presentation:**

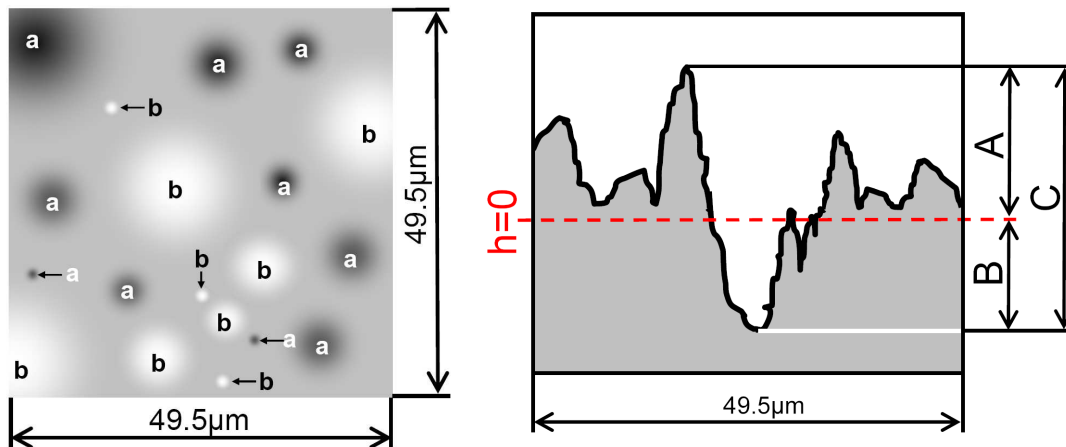


Figure 32. 2D- topographic image (1) and line graphic image of profile (2)

Image 1: a- top places; b- bottom places; **Image 2:** h-referent line; A-distance between the highest point and the basic (referent) line; B- distance between the referent line and the lowest point; C- distance between the highest (top) and the lowest (bottom) points.

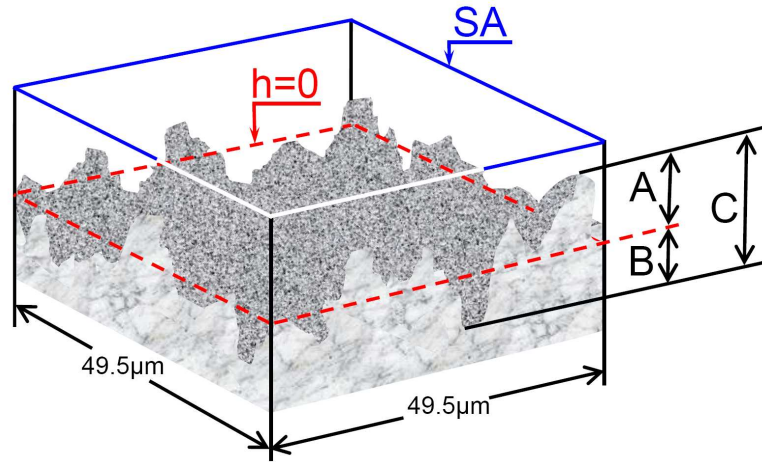


Figure 33. 3-Dimensional surface image

The signatures (A,B,C and h) are the same as in the figure 32, SA- is the surface area measured, and **h**-is basic (referent plane)

• **Roughness measures and values:**

For the scratched samples, the data were obtained in relatively near to the edge of the scratch. The following parameters for evaluation of the roughness rate were used:

✓ *S_a – Roughness average value:*

It is defined by the average sum of the distances of all points from the measured surface, in direction-perpendicular to the conditional plane (parallel to the surface). These distances are represented by module of the corresponding value (it is not taken under attention if the corresponding point is under or above the plane). It is defined by:

$$S_a = \frac{1}{MN} \sum_{k=0}^{M-1} \sum_{l=0}^{N-1} |z(x_k, y_l)| \quad (28)$$

✓ *S_m - Roughness Mean value:*

It also is defined by average sum of the distances of all points from the measured surface, in direction-perpendicular to the conditional plane (parallel to the surface). But in that case the positive or negative value of the direction of the vectors (from the corresponding point to the plane) is also determined. It is defined by equation (29) :

$$S_m = \frac{1}{MN} \sum_{k=0}^{M-1} \sum_{l=0}^{N-1} z(x_k, y_l) \quad (29)$$

✓ *S_q – Root Mean Square value:*

It also is defined by average sum of the distances of all points from the measured surface, in direction-perpendicular to the conditional plane (parallel to the surface). It is defined by:

$$S_q = \sqrt{\frac{1}{MN} \sum_{k=0}^{M-1} \sum_{l=0}^{N-1} z^2(x_k, y_l)} \quad (30)$$

✓ *S_v – The valley depth:*

The value of the distance between the conditional plane and the lowest (bottom) point of the measured surface.

✓ *S_p – The peak height:*

It is the value of the distance between the highest (top) point of the measured surface, and the conditional plane.

✓ *S_y – The Peak – Valley Height:*

It is the distance between the highest, and the lowest points of the measured surface.

$$S_y = S_p - S_v \quad (31)$$

2. Aims of the study:

The basic purpose of the present research work is to compare the results obtained, regarding the performance of protective primer-coatings by application of model equivalent circuits for analysis of electrochemical impedance spectra. The results obtained by Electrochemical Impedance Spectroscopy (EIS) were analyzed by means of modeling, performed via fitting of the respective spectra with appropriated equivalent circuits, and posterior description of the processes observed during the exposure of the samples in a model corrosive medium.

II. EXPERIMENTAL

1. Objects of research

1.1. Influence of the inhibitor's addition to hybrid primary coatings

The objects of research are two samples of AA2024 alloy coated by environmentally friendly hybrid primer-coatings. The expected outcome of the present research is to assess the impact of the concentration of the corrosion inhibitor involved into the primer coating.

Both of samples were composed by AA2024-T354 substrates, coated by surface layers with the following compositions:

(i)- **Sample CIH2:** basic hybrid matrix with addition of 2% wt. of CeCl_3 ; thickness 20.2 μm .

(ii)- **Sample CII2:** basic hybrid matrix prepared by addition of 4% wt. of CeCl_3 , thickness 23.6 μm .

1.2. Effect of the approach applied for inhibitor's addition to hybrid nano-composite primary coatings

(iii)- **Sample CIA6:** basic hybrid matrix with addition of 2% wt. of CeCl_3 , preliminary incorporated in 8% of Al_2O_3 , thickness 12.56 μm .

(iv)- **Sample CIB1:** basic hybrid matrix prepared by addition of 4% wt. of CeCl_3 preliminary incorporated in 8% of Al_2O_3 13.99 μm .

The present research is based on analysis of results obtained by Electrochemical Impedance Spectroscopy, by equivalent circuits modeling procedure. The EIS measurements were performed previously, according to the activities of laboratory LAMAR related to the frame of 6-th Framework Program – IP project **NMP3-CT-2005-**

011783 - MULTIPROTECT.

The EIS spectra were acquired subsequently, after certain periods of time during the exposure of the respective samples into model corrosive medium of 3% solution of NaCl in distilled water (30.0807 grams of NaCl in 1000ml water). The total duration of exposition of the samples into the corrosive medium was predetermined by their durability (the time between the initial moment of exposure and the break-down of the respective sample). Hence, the total exposition for the sample CIH2 was – 175 days (4200 hours), and for the sample CII2 it was – 104 days (2496 h), respectively.

2. Materials and methods:

2.1. Preparation of hybrid nano-composite coatings

The samples of AA2024, coated by the corresponding hybrid and hybrid nano-composite primer coatings were prepared following the sol-gel route.

1. Initially, the hybrid matrix was prepared by mixing together of three sol-gel solutions, as follows:

1.1. For obtaining of organic bridging part: 2,2'-bis-(4-hydroxyphenyl)-propane (BPA), was dissolved in 2-(isopropoxy) ethanol as an organic solvent in 1:2 molar ratio.

1.2. For creation of the inorganic part of the hybrid matrix: a mixture of tetraethyl orthosilicate (TEOS), methyltriethyl orthosilicate (MTEOS) and addition of SiO₂ nanoparticles, as components of the inorganic network, catalysed by concentrated hydrochloric acid (HCl).

1.3. To form the cross linking between the organic substructure and the inorganic network, 3-glycidoxypropyltrimethoxysilane (GPTS) was used. To assist hydrolysis, 0.1 M hydrochloric acid was added as a catalyst.

After the completion of the hydrolysis process, all of these three solutions were mixed together. The procedures for the preparation of the hybrid matrix are described in detail [57], and they are also object of patents [58].

2. The loaded alumina nano-containers were made according to the procedure described in [59].

Shortly, alumina powder (specific surface area 111 m²/g, AluOx C, Degussa (now Evonik, Germany)) was washed hydrochloric acid free. The inhibitor was solved in water in the specific amounts and alumina was added. After 10h of stirring the particles were freeze dried. For redispersion polyvinylbutyral was added together with ethanol. After 12 h stirring and 30 min ultrasound treatment in an ice bath the redispersed particles were characterised and the loading was determined after centrifugation at 20000rpm by HPLC analysis of the supernatant.

3. Before the deposition, the metal plates AA2024 were chemically treated, by weakly alkaline solutions, as described in detail [57 - 59].

All the hybrid and hybrid – nanocomposite primer coatings were synthesized and subsequently deposited, via dip-coating at the Leibniz Institut für Neue Materialien GmbH, Saarbrücken, Germany, using the above described technology [57]. The work team from the Leibniz Institut für Neue Materialien GmbH, Saarbrücken, Germany is greatly acknowledged by the author of the present research work, for the delivery of the samples.

2.2. Brief description of the measuring procedure

The spectra were recorded by use of potentiostat-galvanostat AUTOLAB - PGSTAT 30/2, product of ECOCHEMIE – Netherlands, supported by Frequency Response Analyser FRA 2 unit.

It was connected to three-electrode electrochemical flat cells, with volume of 100 ml. of 3% NaCl solution. Its construction is represented in Figure 34.

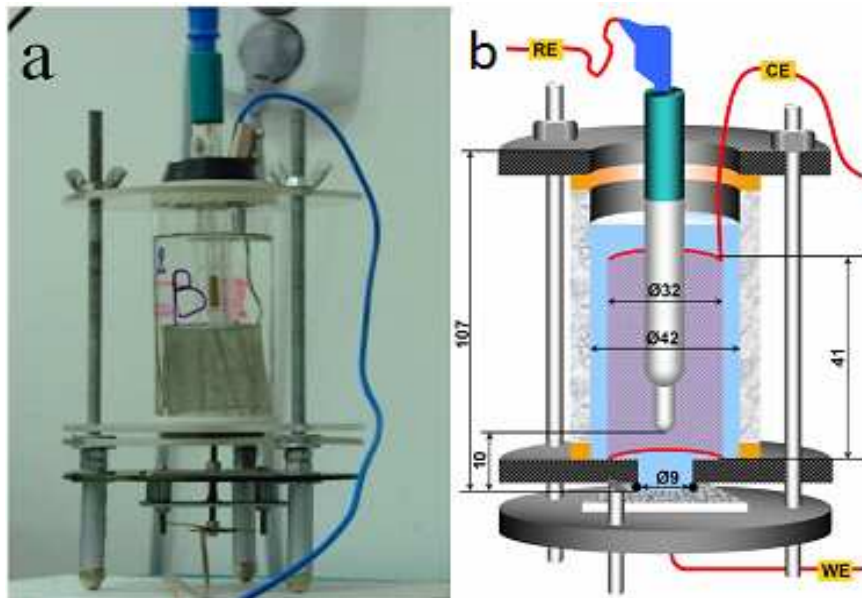


Figure 34. Photography (a) and schematic image (b) of three-electrode electrochemical cell

The simultaneous presence of three-electrodes in the cell enables to enclose two kinds of electric chains, as follows: RE - WE – electric chain for all of the OUTPUT signals from the cell to device, (measured signals), and CE – WE encloses the electric circuits for all of the INPUT signals from the device to the cell (excitation signals). In this assembly, localized areas of the surfaces of the samples objected to measurements serve as working electrodes (WE). For the present measurements, circus zones with area equal to 0.64cm^2 were exposed to the corrosive medium. The counter electrode in that assembly was performed by platinum net with at least two orders of magnitude higher developed surface area, in comparison to this of WE. This relation between the surfaces of WE, and CE in order to avoid any influence of the capacitive resistance of the electric double layer on the surface of CE over the shape of the EIS spectra, during the respective measurements. The reference electrode RE was a standard Ag / AgCl, 3M KCl electrode, model 6.0733.100, product of Metrohm (Netherlands).

2.3. Topographic observations

They were performed by AFM “EasyScan 2” produced by “Nanosurf” (Switzerland).
The conditions of measurements were as follows:

- Square area with linear size 49.5 μm , its surface area is equal to 2.459 nm^2
- Resolution equal to 256 points per line.
- Imaging rate of 1 second per line.
- Measurement mode “scan forward”
- Scan mode from down to up.
- Dynamic regime
- The cantilever used was TAP 190 G, product of Budgetsensors (Bulgaria).

The figure below represents photography of the AFM unit.

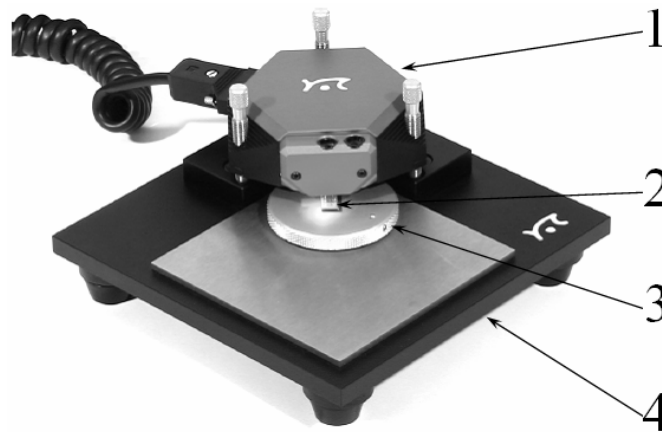


Figure 35. Photography of the AFM measurement unit

1- working head, with the cantilever and the moving mechanism; 2- sample,
3- sample-holder, 4- table

III. RESULTS AND DISCUSSIONS:

1. Model equivalent circuits used for fitting of the spectra:

1.1. Equivalent circuit applied for description of the systems of direct addition of corrosion inhibitor into the corrosive medium

For the needs of the present work, the obtained electrochemical impedance spectra were analyzed using imaginable equivalent circuits, which correspond to the behavior of the respective real electrochemical systems. Figure 36 shows the selected equivalent circuit used for the experiments and modeling procedure.

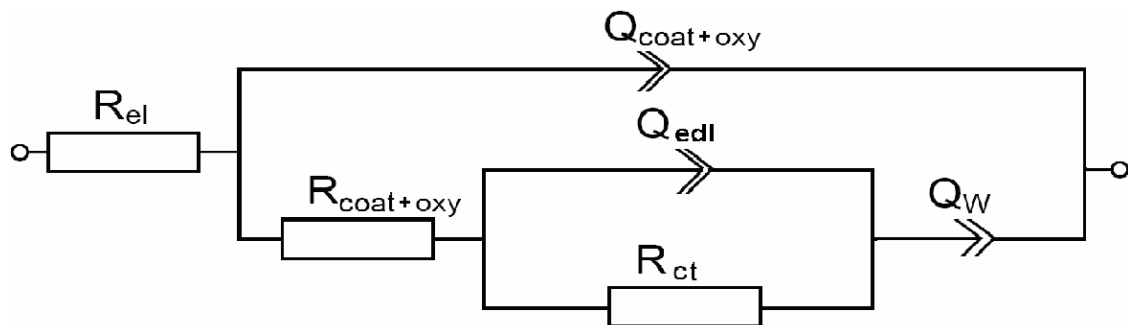


Figure 36. Equivalent circuit for employed for modeling of the entire behavior of the coated system

The behavior of the coated systems during their exposure into the corrosive medium was analysed by application of the depicted above equivalent circuit. The last one, was composed by two time constants. This equivalent circuit is more relevant to the circuits composed by three time constants. According to ref. [21, 25] the hybrid matrix forms covalent bonds to the surface native oxide layer of the Al substrate matrix. Having in account the presence of these bonds, it was assumed that the hybrid coating and the oxide layer are indistinguishable, and there is not any clearly formed interface between them. As a confirmation of this assumption, a visual description [60] of the conjunction between the oxide layer and the hybrid primer coating is shown in Figure 37. The coating

is composed by hydrated silica, bridged by organic moieties and the surface oxide layer of the Al substrate.

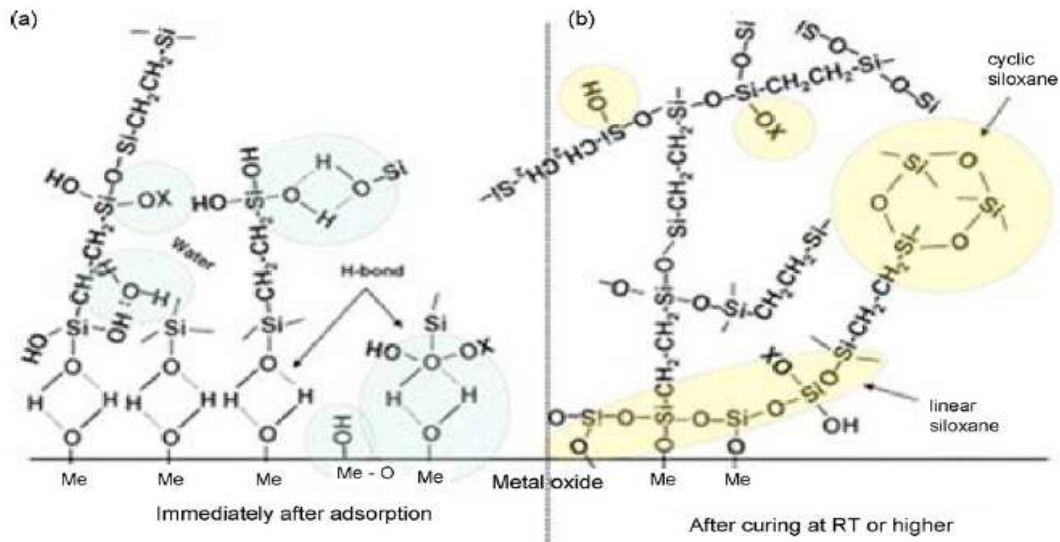


Figure 37. Simplified schematic of bonding mechanism between silane molecules and metal surface hydroxide layer (a) before condensation: hydrogen-bonded interface; (b) after condensation: covalent-bonded interface [60]

The figure represents a clear image of the interactions between the surface oxide layer, and the hybrid primer coating. These interactions are converted from weak hydrogen bonds to strong covalent bonds, during the coating deposition process and subsequent annealing. The covalent bonds form -Al-O-Si- bridges, and consequently it is not possible to arise a clearly definable interface between the oxide layer and hybrid matrix.

Nevertheless, other authors [61] have describes the oxide layer as composed by various oxide – hydroxide minerals, which structure and composition definitely depend from the methods applied regarding thermal treatment. Their investigations were an additive reason to accept that there is not clearly defined interface between the surface oxide layer and the hybrid matrix.

Based on the assumption for absence of clear distinguishable interface a model equivalent circuit with two time constants, instead of the usually used three unit circuit, was selected.

In the above equivalent circuit (Fig. 36), two time constants are used. The first one is related to the resistance of the electrolyte in the pores and defects ($R_{\text{coat+oxy}}$), represented in both of the coating and the oxide layer and the capacity of the of the respective layers by themselves $C_{\text{coat+oxy}}$. The other one, is related to R_{ct} and C_{edl} , namely related to the capacitance of electric double layer and the resistance of the charge transfer reactions in a corrosion process. The reactions are going on between the components of the metal surface and these species of the electrolyte, which overcame the potential barrier of the double layer.

Before the breakdowns of the coatings all of the impedance spectra represented only one depressed semi-circle in Nyquist plots, and only one large picks in the corresponding Bode plots. It was accepted that they were composed by two overlapped time constants. The overlapping is possible only when the both of capacitive elements $C_{\text{coat+oxy}}$ and C_{edl} have values from the same order of magnitude.

In the both of equivalent circuits the pure capacity, is substituted by Constant Phase Element (Q) because the phase shift (φ) is lower than 90° . The parameter Q is related to the frequency ω by the following equation:

$$Q = \frac{1}{Y_0} (j\omega)^{-n} \quad (32)$$

where: Y_0 and n are constants. When the values of n are in the range $0.8 < n \leq 1$, the parameter Y_0 has the meaning of capacity and its values are in Farad.

Other specific feature of this equivalent circuit is the modeling of the diffusion process by Constant Phases Element (Q_w), instead of a Warburg element. This substitution is reasonable when the diffusion processes are hindered by presence of hydrodynamic barriers, such as filter layers, for example.

After prolonged exposition (individual for every sample), new time-constant appears. It is a contribution of the substrate's corrosion. Its appearance is evidence for the failure of the protective ability of the corresponding coating. The coatings can not perform their protective role, after the moment of substrate's corrosion appearance.

2. Results obtained after fitting of the experimental data to the appropriated equivalent circuits

2.1. Results for the sample with 2% CeCl₃:

Results obtained from the impedance spectra fitting procedure of CIH2 sample are as follows:

Table 3. Results obtained for the first 13 days of exposure for sample CI H2

CI H2	Sample CI H2 initial period									
	1h		D2		D4		D7		D13	
	Value	χ^2	Value	χ^2	Value	χ^2	Value	χ^2	Value	χ^2
R1[$\Omega \cdot \text{cm}^2$] $\times 10^3$	-0.91	12.8	-0.94	8	-1.32	3.8	-1.02	5.8	-1.01	4
Q1[$\text{s}^n \cdot \Omega^{-1} \cdot \text{cm}^2$] $\times 10^{-9}$	0.596	5.4	0.567	2.7	0.545	1.8	0.572	2	0.549	1.2
n[/]	0.95	0.5	0.95	0.3	0.959	0.2	0.96	0.2	0.958	0.1
R2[$\Omega \cdot \text{cm}^2$] $\times 10^6$	2.71	12	5.90	7.8	10.13	7.5	8.99	6.5	15.95	6.1
Q2[$\text{s}^n \cdot \Omega^{-1} \cdot \text{cm}^2$] $\times 10^{-8}$	0.353	14.2	0.457	8.3	0.464	6.9	0.582	8.8	0.496	6.1
n[/]	0.734	5	0.673	3.9	0.611	3.6	0.646	4.6	0.577	3.5
R3[$\Omega \cdot \text{cm}^2$] $\times 10^6$	4.90	7.2	10.14	5.1	17.01	5	10.6	6.2	24.53	4.6
Q3[$\text{s}^n \cdot \Omega^{-1} \cdot \text{cm}^2$] $\times 10^{-5}$	0.209	4.7	0.196	4.9	0.195	5.1	0.192	4.2	0.201	5
n[/]	0.791	1.5	0.821	1.4	0.851	1.4	0.855	1.2	0.91	1.3

Table 4. Results obtained for the intermediated period of exposure for sample CI H2

CI H2	Sample CI H2 later period									
	D27		D32		D42		D48		D63	
	Value	χ^2	Value	χ^2	Value	χ^2	Value	χ^2	Value	χ^2
R1[$\Omega \cdot \text{cm}^2$] $\times 10^3$	-0.814	6.1	-1.089	5.1	-0.757	4.2	-0.79	8.3	-0.78	4.3
Q1[$\text{s}^n \cdot \Omega^{-1} \cdot \text{cm}^2$] $\times 10^{-9}$	0.561	1.7	0.569	2.1	0.573	1.3	0.5714	2	0.573	1.5
n[/]	0.959	0.2	0.9594	0.2	0.96	0.1	0.9604	0.2	0.961	0.2
R2[$\Omega \cdot \text{cm}^2$] $\times 10^6$	12.04	7.9	9.03	9.4	7.62	8.9	10.5	18	9.39	5.4
Q2[$\text{s}^n \cdot \Omega^{-1} \cdot \text{cm}^2$] $\times 10^{-8}$	0.664	8.7	0.744	10.9	0.869	8.2	0.8396	14	1.109	6.2
n[/]	0.566	4.9	0.569	5.9	0.49	4	0.4415	7.7	0.385	2.5
R3[$\Omega \cdot \text{cm}^2$] $\times 10^6$	16.28	6.6	11.27	8.4	12.06	6.2	20.37	10.7	20.45	12.2
Q3[$\text{s}^n \cdot \Omega^{-1} \cdot \text{cm}^2$] $\times 10^{-5}$	0.177	5	0.1594	4.5	0.179	2.4	0.165	5.8	0.19	5.4
n[/]	0.868	1.3	0.833	1.3	0.884	0.6	0.882	1.5	0.923	1.3

Table 5. Results obtained for the final period of exposure for sample CI H2

CI H2	Sample CI H2 final period					
	D69		D79		D84	
	Value	χ^2	Value	χ^2	Value	χ^2
R1[Ω .cm ²] $\times 10^3$	-0.764	8.6	-0.749	9.6	Corrosion	
Q1[sn. Ω -1.cm ²] $\times 10^{-9}$	0.59	2.8	0.592	2.6	Corrosion	
n[/]	0.959	0.3	0.959	0.3	Corrosion	
R2[Ω .cm ²] $\times 10^6$	12.04	17.7	10.17	17.2	Corrosion	
Q2[sn. Ω -1.cm ²] $\times 10^{-8}$	0.661	19.1	1.701	17.6	Corrosion	
n[/]	0.566	11.6	0.42	13.9	Corrosion	
R3[Ω .cm ²] $\times 10^6$	16.28	15.7	14.35	15.8	Corrosion	
Q3[sn. Ω -1.cm ²] $\times 10^{-5}$	0.177	5.1	0.163	7.8	Corrosion	
n[/]	0.868	1.4	0.894	2	Corrosion	

Graphical results obtained for the sample with 2% CeCl₃ are shown in Figures 38 and 39.

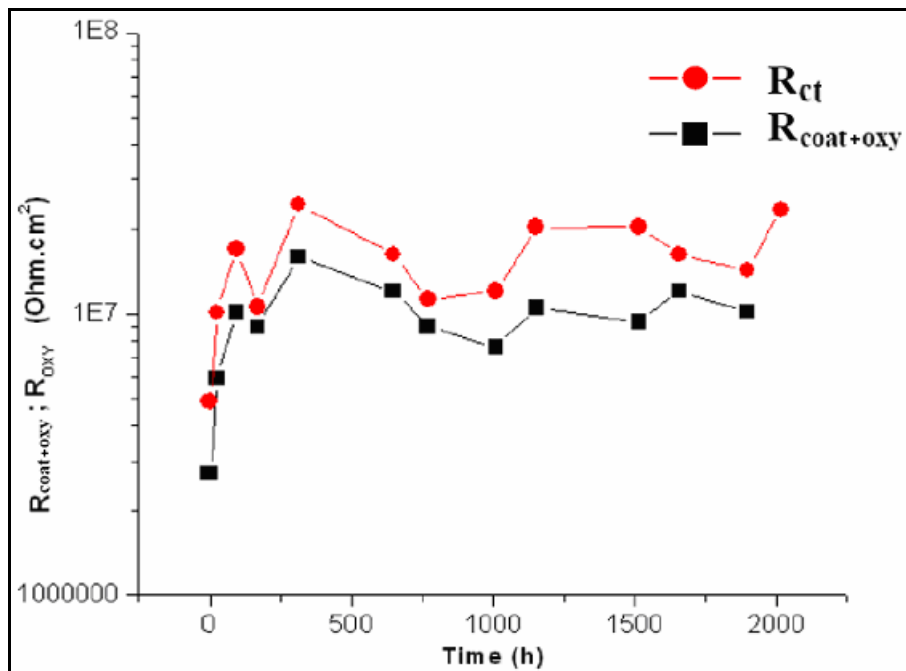


Fig 38. Evolution of the Ohmic resistances of: intermediate oxide layer (R_{ct}), and the coating ($R_{coat+oxy}$), of sample H2

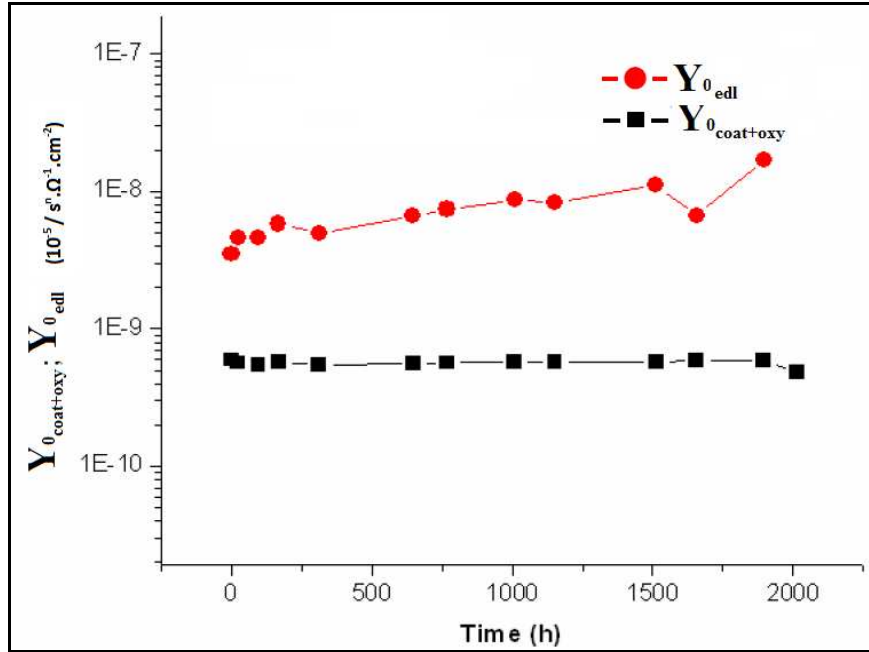


Fig 39. Evolution of the values of the constant Y_0 for: intermediate oxide layer (Y_{0_edl}), and the coating ($Y_{0_coat+oxy}$), of sample H2

2.2. Results for the sample with 4% $CeCl_3$:

Tabular results obtained from the fitting of the impedance spectra for CI12 sample are presented in Tables 6 and 7.

Table 6. Results obtained for the initial period of exposure for sample CI I2

CI I2	Sample CI I2 initial period									
	2h		D2		D4		D7		D13	
	Value	χ^2	Value	χ^2	Value	χ^2	Value	χ^2	Value	χ^2
$R1[\Omega.cm^2] \times 10^3$	-1.137	23.0	-1.219	7.6	-0.783	4.3	-1.01	8.3	-1.15	4.3
$Q1[s^n \cdot \Omega^{-1} \cdot cm^2] \times 10^{-9}$	0.479	0.7	0.492	2.7	0.88	1.6	0.531	2.9	0.503	1.5
n[/]	0.949	0.7	0.9509	0.3	0.935	0.2	0.9494	0.3	0.957	0.2
$R2[\Omega.cm^2] \times 10^6$	6.36	16.4	6.96	6.9	5.26	0.6	5.12	7.8	10.3	5.4
$Q2[s^n \cdot \Omega^{-1} \cdot cm^2] \times 10^{-8}$	0.228	45.9	0.515	13.9	0.38	6.6	0.529	18.6	0.431	6.2
n[/]	0.839	15.15	0.708	6.0	0.686	2.7	0.7183	7.1	0.662	2.5
$R3[\Omega.cm^2] \times 10^6$	4.61	24.4	5.86	8.8	8	4.6	3.36	12.5	6.81	4.3
$Q3[s^n \cdot \Omega^{-1} \cdot cm^2] \times 10^{-5}$	0.97	10.5	0.174	3.6	0.149	1.6	0.174	2.5	0.138	1.4
n[/]	0.638	4.1	0.842	1.1	0.87	0.5	0.854	0.7	0.86	0.4

Table 7. Results obtained for the final period of exposure for sample CI I2

CI I2	Sample CI I2 final period									
	D27		D32		D48		D63		D71	
	Value	χ^2	Value	χ^2	Value	χ^2	Value	χ^2	Value	χ^2
$R1[\Omega.cm^2]x10^3$	-0.993	6.7	-1.02	11.9	-0.964	6.5	-0.976	6.1	Corrosion	
$Q1[s^n.\Omega^{-1}.cm^2]x10^{-9}$	0.522	2.4	0.545	4.5	0.532	2.4	0.547	2.2	Corrosion	
n[/]	0.952	0.2	0.951	0.4	0.954	0.2	0.953	0.2	Corrosion	
$R2[\Omega.cm^2]x10^6$	6.36	8.0	5.01	11.9	6.77	9.7	6.77	8.4	Corrosion	
$Q2[s^n.\Omega^{-1}.cm^2]x10^{-8}$	0.347	20.5	0.33	45.3	0.392	27.7	0.373	24.6	Corrosion	
n[/]	0.744	6.9	0.834	13.8	0.719	8.5	0.739	7.7	Corrosion	
$R3[\Omega.cm^2]x10^6$	3.73	14.6	2.04	30.0	3.3	20.4	3.27	17.9	Corrosion	
$Q3[s^n.\Omega^{-1}.cm^2]x10^{-5}$	0.164	2.1	0.146	3.3	0.162	1.9	0.157	1.8	Corrosion	
n[/]	0.864	0.6	0.813	1.0	0.875	0.6	0.877	0.5	Corrosion	

Figures 40 and 41 show time dependence obtained for the sample with 4% CeCl₃.

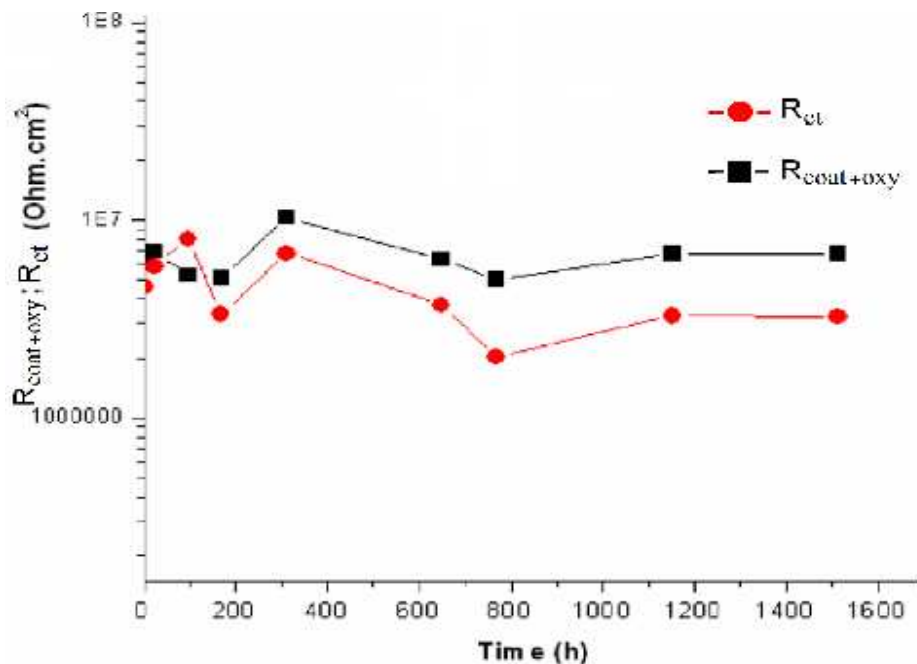


Fig 40. Evolution of the Ohmic resistances of: intermediate oxide layer (R_{ct}), and the coating ($R_{coat+oxy}$), of sample I2

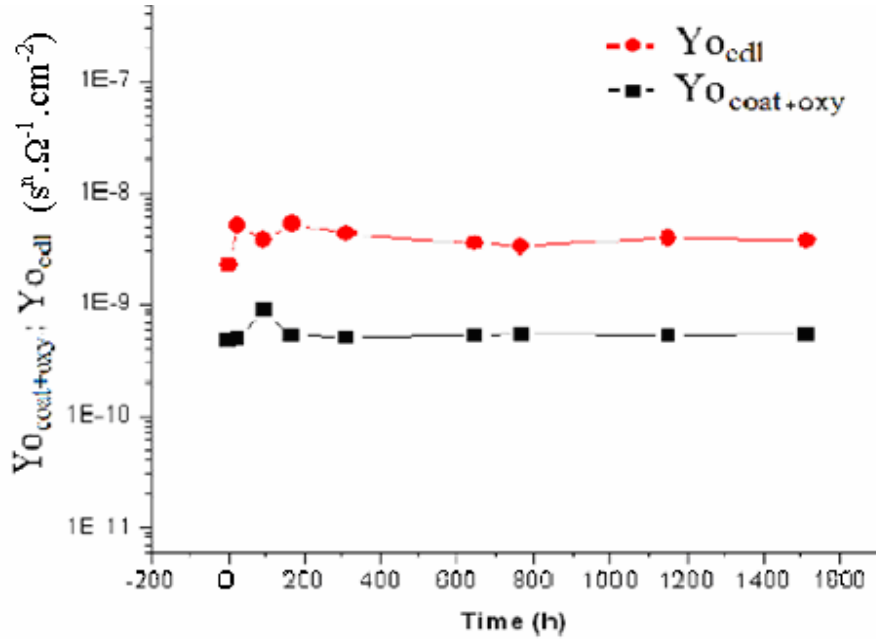


Fig 41. Evolution of the values of the constant Y_0 for: intermediate oxide layer ($Y_{0_{cdl}}$), and the coating ($Y_{0_{coat+oxy}}$), of sample I2

2.3. Results for the sample with 2% $CeCl_3$ preliminary incorporated in 8% Al_2O_3 nano-particles:

In Tables 8, 9 and 10 are presented results obtained from the fitting of the impedance spectra for the sample CI A6 (with 2% $CeCl_3$, incorporated in 8% Al_2O_3 nano-particles)

Table 8. Results obtained for the initial period of exposure for sample CI A6

CI A6	Sample CI A6 initial period									
	D2		D5		D6		D8		D13	
	Value	χ^2	Value	χ^2	Value	χ^2	Value	χ^2	Value	χ^2
$R1[\Omega \cdot cm^2] \times 10^3$	-0.555	9.5	-0.563	8.9	-0.543	6.0	-0.532	5.9	-0.61	4.9
$Q1[s^n \cdot \Omega^{-1} \cdot cm^2] \times 10^{-9}$	0.866	3.5	0.852	3.0	0.863	1.9	0.871	1.8	0.863	1.6
n[/]	0.95	0.3	0.952	0.2	0.951	0.2	0.951	0.2	0.952	0.1
$R2[\Omega \cdot cm^2] \times 10^6$	2.777	14.6	4.09	12.1	4.35	7.4	4.15	7.1	6.23	8.2
$Q2[s^n \cdot \Omega^{-1} \cdot cm^2] \times 10^{-8}$	0.679	11.4	0.59	9.1	0.714	5.9	0.808	6.2	0.75	5.6
n[/]	0.615	4.7	0.626	4.2	0.612	2.9	0.606	3.1	0.562	3.1
$R3[\Omega \cdot cm^2] \times 10^6$	5.36	8.1	8.61	6.3	8.51	4.2	7.31	4.5	13.67	4.3
$Q3[s^n \cdot \Omega^{-1} \cdot cm^2] \times 10^{-5}$	0.185	2.5	0.197	3.4	0.202	2.3	0.2	2.1	0.17	3.2
n[/]	0.877	0.7	0.881	0.9	0.88	0.6	0.88	0.6	0.853	0.8

Table 9. Results obtained for the later period of exposure for sample CI A6

CI A6	Sample CI A6 later period									
	D19		D22		D35		D40		D55	
	Value	χ^2	Value	χ^2	Value	χ^2	Value	χ^2	Value	χ^2
R1[$\Omega \cdot \text{cm}^2$] $\times 10^3$	-0.571	9.6	-0.54	5.7	-0.556	5.9	-0.515	6.8	-0.43	6.72
Q1[$\text{s}^n \cdot \Omega^{-1} \cdot \text{cm}^2$] $\times 10^{-9}$	0.863	3.5	0.863	1.8	0.846	2.2	0.89	3.0	1.01	4.1
n[/]	0.952	0.3	0.953	0.2	0.954	0.2	0.952	0.2	0.96	0.4
R2[$\Omega \cdot \text{cm}^2$] $\times 10^6$	5.54	28.5	5.77	12	5.33	26.2	2.83	28.8	1.8	64.5
Q2[$\text{s}^n \cdot \Omega^{-1} \cdot \text{cm}^2$] $\times 10^{-8}$	0.647	12.1	0.812	6.2	0.765	7.3	1.13	13.5	1.01	17.1
n[/]	0.507	6.5	0.509	3.6	0.434	4.4	0.452	5.5	0.432	5.3
R3[$\Omega \cdot \text{cm}^2$] $\times 10^6$	19.4	9.4	16.57	4.9	29.68	5.8	9.09	9.8	10.95	11.4
Q3[$\text{s}^n \cdot \Omega^{-1} \cdot \text{cm}^2$] $\times 10^{-5}$	0.142	9.7	0.171	3.7	0.163	5.7	0.165	2.6	0.16	2.9
n[/]	0.783	2.7	0.86	1.0	0.881	1.4	0.86	0.7	0.875	0.9

Table 10. Results obtained for the last period of exposure for sample CI A6

CI A6	Sample CI A6 final period							
	D63		D82		D97		D125	
	Value	χ^2	Value	χ^2	Value	χ^2	Value	χ^2
R1[$\Omega \cdot \text{cm}^2$] $\times 10^3$	-0.524	6.6	-0.57	6.5	-0.513	7.5	Corrosion	
Q1[$\text{s}^n \cdot \Omega^{-1} \cdot \text{cm}^2$] $\times 10^{-9}$	0.929	3.5	0.923	3.9	0.954	4.9	Corrosion	
n[/]	0.951	0.3	0.95	0.3	0.949	0.4	Corrosion	
R2[$\Omega \cdot \text{cm}^2$] $\times 10^6$	2.065	45.1	2.418	61.1	1.545	65.9	Corrosion	
Q2[$\text{s}^n \cdot \Omega^{-1} \cdot \text{cm}^2$] $\times 10^{-8}$	1.263	14.4	0.937	14	0.112	16.8	Corrosion	
n[/]	0.418	5.8	0.416	5.7	0.428	5.3	Corrosion	
R3[$\Omega \cdot \text{cm}^2$] $\times 10^6$	9.88	10.4	16.57	10	9.6	11.4	Corrosion	
Q3[$\text{s}^n \cdot \Omega^{-1} \cdot \text{cm}^2$] $\times 10^{-5}$	0.159	2.8	0.138	4	0.14	2.6	Corrosion	
n[/]	0.873	0.8	0.867	1.1	0.858	0.8	Corrosion	

Time evolution behaviour for sample with 2% CeCl_3 , incorporated in 8% Al_2O_3 nano-particles, is presented in Figures 42 and 43.

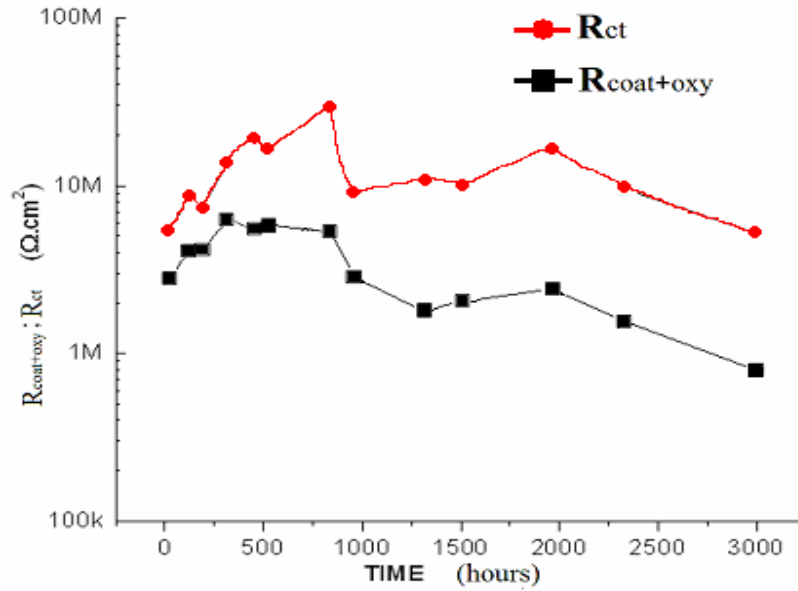


Fig 42. Evolution of the Ohmic resistances of: intermediate oxide layer (R_{ct}), and the coating ($R_{coat+oxy}$), of sample A6

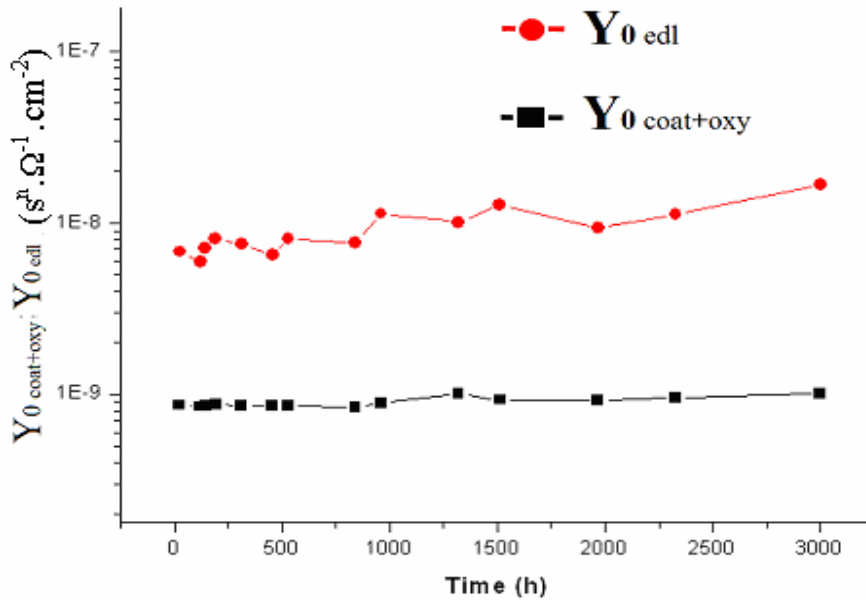


Fig 43. Evolution of the values of the constant Y_0 for: intermediate oxide layer ($Y_{0 \text{ edl}}$), and the coating ($Y_{0 \text{ coat+oxy}}$), of sample A6

2.4. Results for sample with 4% CeCl₃ preliminary incorporated in 8% Al₂O₃ nano-particles:

Tables 11,12 and 13 summarised results obtained from the fitting of the impedance spectra for sample CIB1 (with 4% CeCl₃, incorporated in 8% Al₂O₃ nano-particles)

Table 11. Results obtained for the initial period of exposure for sample CIB1

CIB1	Sample CIB1 initial period									
	30min		D2		D5		D6		D9	
	Value	χ^2	Value	χ^2	Value	χ^2	Value	χ^2	Value	χ^2
R1[$\Omega \cdot \text{cm}^2$] $\times 10^3$	-0.711	8.2	-0.555	5.2	-0.672	5.4	-0.679	5.3	-0.7	5.2
Q1[s ⁿ . $\Omega^{-1} \cdot \text{cm}^2$] $\times 10^{-9}$	0.789	4.0	0.866	2.0	0.751	2.0	0.763	2.0	0.775	2.1
n[/]	0.944	0.4	0.949	0.2	0.949	0.2	0.948	0.2	0.947	0.2
R2[$\Omega \cdot \text{cm}^2$] $\times 10^6$	1.637	11.4	2.778	7.0	3.73	7.1	3.63	7.0	3.46	7.9
Q2[s ⁿ . $\Omega^{-1} \cdot \text{cm}^2$] $\times 10^{-8}$	0.809	19.4	0.679	12.7	0.527	12.5	0.546	12.7	0.544	14.0
n[/]	0.674	6.4	0.615	4.3	0.696	4.3	0.699	4.3	0.688	4.6
R3[$\Omega \cdot \text{cm}^2$] $\times 10^6$	1.374	14.1	5.35	9.2	3.053	9.3	2.877	9.2	2.771	10.1
Q3[s ⁿ . $\Omega^{-1} \cdot \text{cm}^2$] $\times 10^{-5}$	0.172	1.2	0.185	1.2	0.179	1.2	0.18	1.1	0.179	1.2
n[/]	0.879	0.4	0.877	0.3	0.892	0.4	0.892	0.3	0.893	0.4

Table 12. Results obtained for later period of exposure for sample CIB1

CIB1	Sample CIB1 later period									
	D12		D19		D22		D30		D40	
	Value	χ^2	Value	χ^2	Value	χ^2	Value	χ^2	Value	χ^2
R1[$\Omega \cdot \text{cm}^2$] $\times 10^3$	-0.775	4.6	-0.74	5.0	-0.684	7.3	-0.78	9.7	-0.64	6.1
Q1[s ⁿ . $\Omega^{-1} \cdot \text{cm}^2$] $\times 10^{-9}$	0.77	2.0	0.762	2.1	0.769	1.9	0.779	3.8	0.797	3.1
n[/]	0.949	0.2	0.950	0.2	0.949	0.2	0.948	0.4	0.948	0.3
R2[$\Omega \cdot \text{cm}^2$] $\times 10^6$	4.19	8.3	4.56	10.2	3.68	10.4	4.96	14.4	2.212	16.9
Q2[s ⁿ . $\Omega^{-1} \cdot \text{cm}^2$] $\times 10^{-8}$	0.482	14.5	0.464	15.5	0.526	14.6	0.388	27.3	0.68	20.3
n[/]	0.688	4.7	0.662	4.9	0.639	4.7	0.737	9.5	0.597	5.1
R3[$\Omega \cdot \text{cm}^2$] $\times 10^6$	3.41	10.6	4.24	11.3	3.77	10.5	3.79	19.6	2.659	14.4
Q3[s ⁿ . $\Omega^{-1} \cdot \text{cm}^2$] $\times 10^{-5}$	0.176	1.3	0.171	1.5	0.17	1.3	0.124	3.3	0.174	1.1
n[/]	0.891	0.4	0.891	0.4	0.887	0.4	0.776	1.1	0.887	0.3

Table 13. Results obtained for the last period of exposure for sample CI B1

CI B1	Sample CI B1 final period									
	D56		D83		D97		D125		D137	
	Value	χ^2	Value	χ^2	Value	χ^2	Value	χ^2	Value	χ^2
R1[$\Omega \cdot \text{cm}^2$] $\times 10^3$	-0.587	25.5	-0.704	5.4	-0.942	6.8	-0.962	3.5	Corrosion	
Q1[s ⁿ . $\Omega^{-1} \cdot \text{cm}^2$] $\times 10^{-9}$	0.579	66.2	0.872	3.4	0.614	6.0	0.972	3.0	Corrosion	
n[/]	0.974	8.3	0.943	0.3	0.949	0.5	0.937	0.3	Corrosion	
R2[$\Omega \cdot \text{cm}^2$] $\times 10^6$	14.24	100	1.74	21.6	1.39	40.2	0.78	6.5	Corrosion	
Q2[s ⁿ . $\Omega^{-1} \cdot \text{cm}^2$] $\times 10^{-8}$	0.325	69.3	0.121	13.9	0.548	11.1	0.937	5.9	Corrosion	
n[/]	0.59	17.9	0.498	4.5	0.524	2.7	0.664	2.1	Corrosion	
R3[$\Omega \cdot \text{cm}^2$] $\times 10^6$	4.72	39.7	3.97	9.9	8.14	7.2	1.515	3.6	Corrosion	
Q3[s ⁿ . $\Omega^{-1} \cdot \text{cm}^2$] $\times 10^{-5}$	0.166	1.5	0.151	1.2	0.147	1.8	0.157	0.7	Corrosion	
n[/]	0.884	0.5	0.877	0.4	0.877	0.6	0.874	0.2	Corrosion	

Figures 44 and 45 show results obtained from the fitting of the impedance spectra for the sample CIB1 (with 4% CeCl₃, incorporated in 8% Al₂O₃ nano-particles)

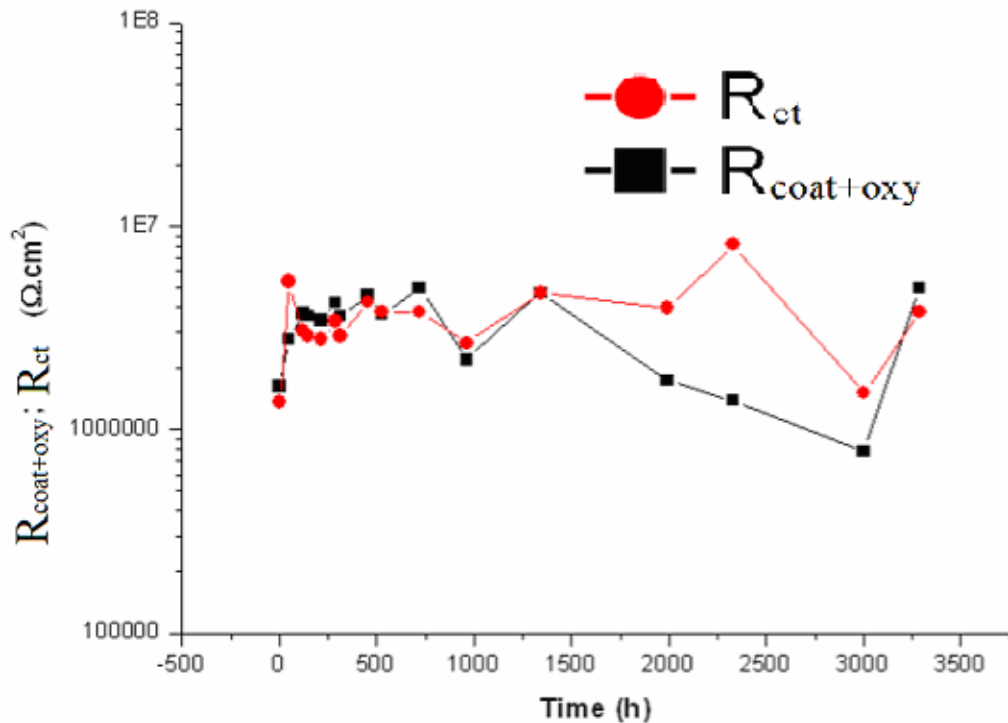


Fig 44. Evolution of the values of the constant Y_0 for: intermediate oxide layer (Y_{0ct}), and the coating ($Y_{0coat+oxy}$), of sample B1

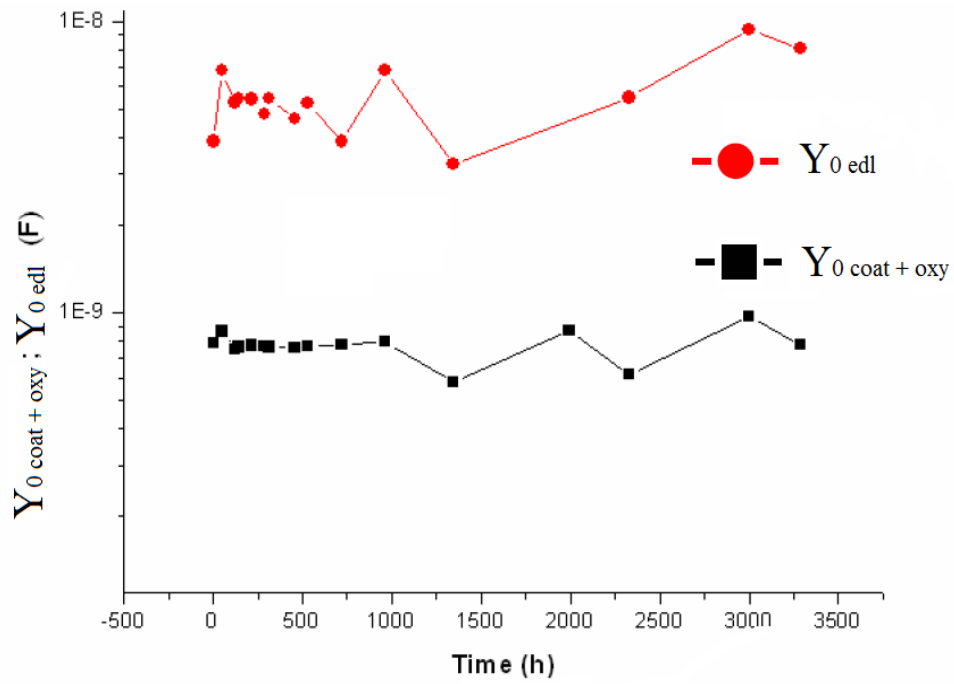


Fig 45. Evolution of the values of the constant Y_0 for: intermediate oxide layer ($Y_{0 \text{ edl}}$), and the coating ($Y_{0 \text{ coat+oxy}}$), of sample B1

IV. DISCUSSION ABOUT THE RESULTS OBTAINED BY MODELING

1. Discussions over the evolution of the impedance parameters for the hybrid primer coatings.

All of the impedance spectra reveal almost the same shape. At the high frequency's range of the spectra, completely capacitive behavior is represented. This behavior is related to the coating capacity. At lower frequencies part (from 0.1 to 10Hz) an additive resistive compartment appears, originated from the resistance of the electrolyte in the pores of the coating. Specific feature of all of the spectra is that a straight line is represented in the Nyquist plot at the lowest frequency's range. The

relation between the imaginary and the real component of the impedance $\frac{\Delta Z''}{\Delta Z'}$ possess constant value. This mathematic relationship is expression of diffusion limits which retard the entire corrosion process. Figures 46 and 47 show superposition of three impedance spectra, acquired for three different periods of exposure for sample CI H2.

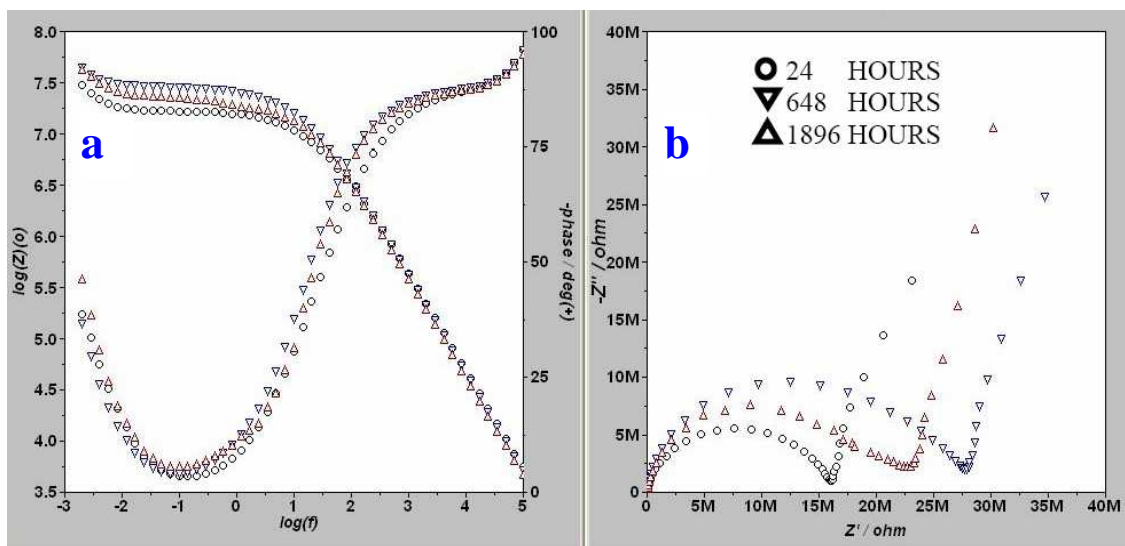


Fig 46. Evolution of the impedance spectra of coating H2, Bode (a); and Nyquist (b) plots

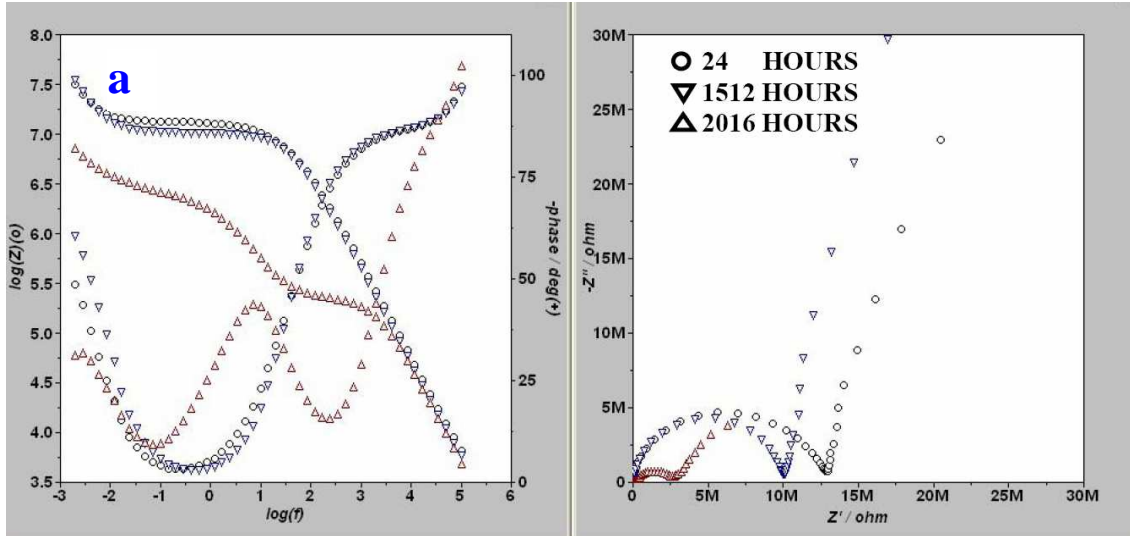
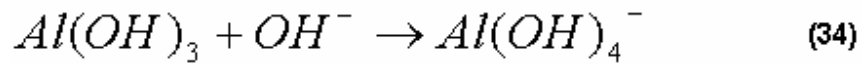
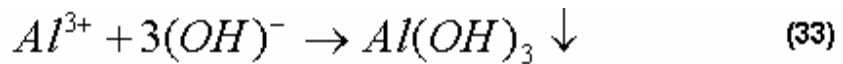


Fig 47. Evolution of the impedance spectra of coating I2, Bode (a); and Nyquist (b) plots

According to some authors, these limits could be originated from either to hindered diffusion of hydroxyl ions towards the metal surface, or the hindered diffusion of $Al(OH)_4^-$ ions, which are produced by the following reactions:



It should be mentioned that after an undefined period of time exposition into the corrosive medium the impedance spectra undergo to a sharp change. New maximum appears in the range of 10Hz, in the phase shift diagrams of the respective Bode plots. It reveals, simultaneously with a new inflexion of the respective $\log [Z]$ at the same frequency range. At the same time, the corresponding Nyquist plots also suffer sharp changes. At the highest frequency range, new clearly distinguishable semicircle appears. These changes are indication for occurrence of completely new processes, such as intergranular corrosion for instance.

Figure 48 shows the impedance spectra of both of samples after the failure.

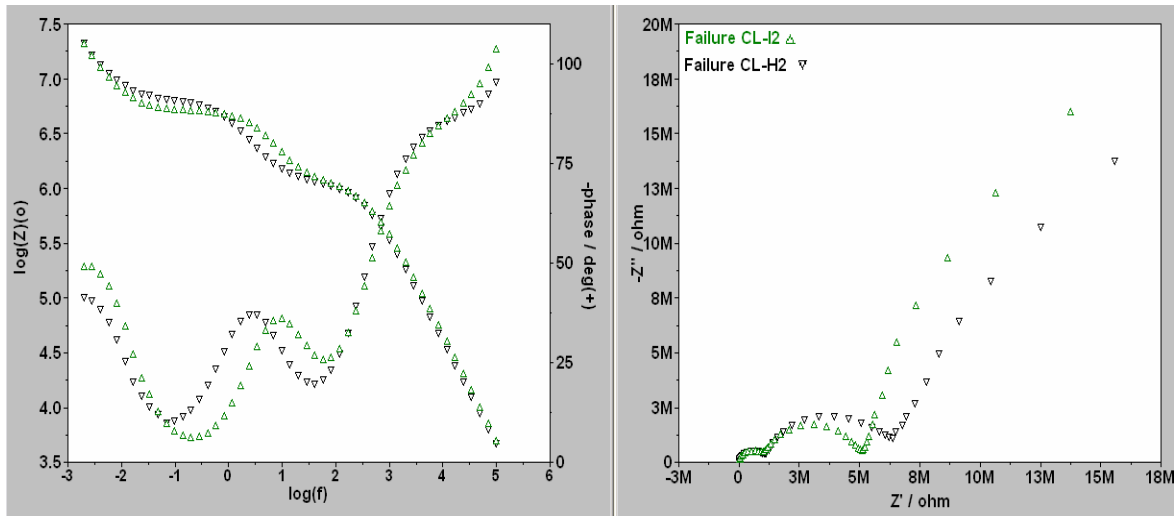


Figure 48. Examples for impedance spectra of the coatings after their failures

The period expensed since the first moment of exposition of the respective sample to the described above failure could be described as *durability of the coating*. It is individual for each coating, and could be used as a measure for characterization of the passive corrosion protective ability of the investigated coatings. According to this measure, CIH2-coating with 2% CeCl_3 addition excels this one with the higher inhibitor's content (CII2), because for the former sample the durability is equal to 79 days (1896 hours), while for the latter, it is only 63 days (1512 hours). After these treatment periods, the impedance spectra could not be properly fitted by the equivalent circuit, represented in Figure 36. According to Zheludkevich [62, 63] the spectra should be fitted using another equivalent circuit, as the author is demonstrated in the respective publications.

2. Discussions over the evolution of the impedance parameters for the hybrid nano-composite primer coatings

Generally, the hybrid nano-composite primer coatings (97 days for sample CIA6 and 125 days for CIB1, respectively) reveal higher level of durability than the hybrid ones (CIH2 and CII2). That result confirms the suggestion of Lamaka [44], that the nano-particles supply a gradual release of the corrosion inhibitor, which enables an additive extension of the durability of the respective primer coatings.

In addition, both $R_{\text{coat+oxy}}$ and R_{ct} values for the sample CIA6, with 2% of inhibitor, is in three orders of magnitude higher to comparison to sample CIB1, with 4% CeCl_3 at the moment before the breakdown of both coatings. It seems that in the case of higher inhibitor's content (CIB1 sample) the coating possesses higher barrier ability, but it loses it relatively earlier than CIA6 sample (see dependences in Figures 42 and 44).

3. Protective ability of the hybrid and the hybrid nano-composite coatings

Undoubtedly, due to the application of completely different approaches for the introduction of the inhibitor into the coating systems, the obtained samples have different behaviors. It was the reason to perform a comparative analysis of their behaviors during their exposure into the corrosive medium. The analysis was performed after fitting of the impedance spectra to appropriated equivalent circuit (as commented before).

If the impedance spectra of the corresponding samples, acquired after different periods of exposure are overlapped, than a visual image for the evolution of the electrochemical parameters could be achieved. Figure 49 shows impedance spectra of a hybrid CIH2 coating- (b) and the hybrid nano-composite CIA6- (a) coating, both recorded after different periods i.e. from 24h to 1968 h exposure time.

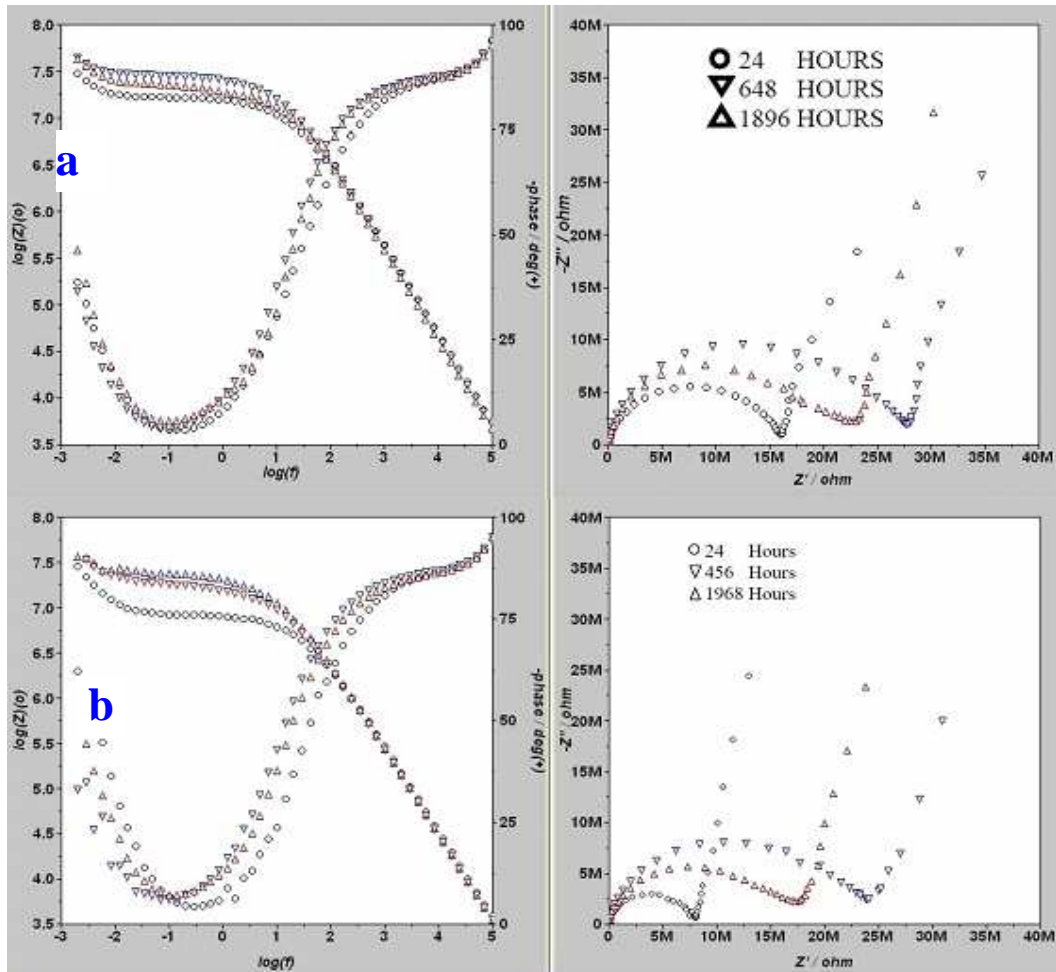


Figure 49. Impedance spectra recorded after different exposure times

The figure shows that all of the spectra possess similar shapes, which is the reason to apply the same equivalent circuit for both of the investigated samples.

After certain extend of exposure, a sharp change of the shape of the impedance spectra is observed. That sharp change is indication for the failure of the coating. Namely, the sample changes entirely its behavior. New maxima arise in the Bode plots, simultaneously with remarkable decrease of the semicircles in the Nyquist plots.

The time between the first moment of exposition of the sample and the moment of the coating failure could be applied as a measure for the *durability* of the coatings.

Tables 7 and 10 show that the hybrid primer coating is less durable than the nano-composite one. The coating of sample CIA6 breaks down after 97 days of exposure, while for sample CIH2 this period is 79 days, only.

Figure 50 shows the evolution of the resistances of the coating and the charge transfer (corrosion) reactions.

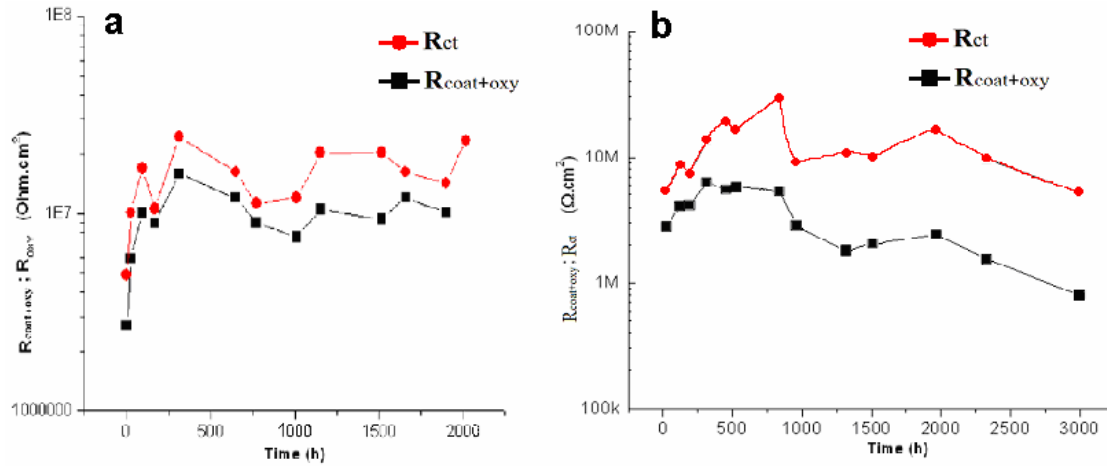


Figure 50. Evolution of the resistances of $R_{coat+oxy}$ and R_{ct} for the hybrid (a) and the hybrid nano-composite (b) coatings

The resistances of the electrolyte penetrated in the pores of the coating $R_{coat+oxy}$ and the resistance of the charge transfer reactions R_{ct} (R2 and R3 on the tables, respectively) are the basic indicator for the barrier ability of the coatings. It was established that the values of $R_{coat+oxy}$ for the hybrid coating are in the range of 2 to 15 M Ω , achieving their maximal value checked at 13 day of exposure. The resistance of the hybrid nano-composite coating has relatively lower values. They correspond to relatively lower barrier ability for the sample containing nano-particles. This weak negative effect is compensated by the prolonged durability as was marked above. Both of lower barrier ability and higher durability for CIA6 indicate that the nano-particles gradually release the inhibitor from their bulk. In the case of the direct addition of inhibitor to the hybrid matrix, it looks that the coating suffers a sharp break down, probably triggered by the dissolving of the inhibitor's salt. It means that the direct addition of the inhibitor into the hybrid matrix has a detrimental effect over the stability of the coating. This effect is suppressed when the inhibitor is previously impregnated in the nano-particles. The constant phase elements which correspond to the capacitances of the coatings $Y_{0\ coat+oxy}$ do not change during the exposition of the samples. It seems that the penetration of electrolyte almost does not influence over their capacity. This fact is expectable, because

the relative static permittivity of the hybrid matrix, (ϵ_R), equal to 60 – 90 has relatively near values to these of the water (80 – 88).

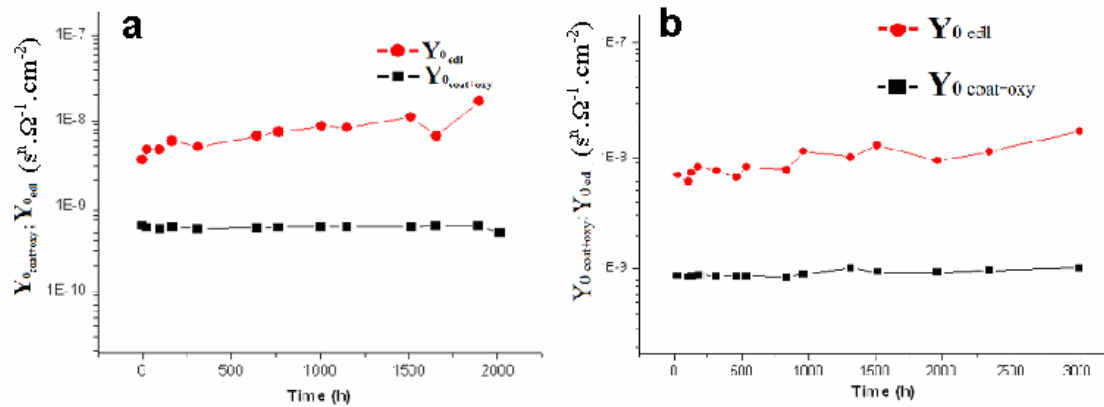


Figure 51. Evolution of the resistances of $Y_{0\text{coat+oxy}}$ and $Y_{0\text{edl}}$ for the hybrid (a) and the hybrid nano-composite (b) coatings

The $Y_{0\text{edl}}$ values suffer an increase, but they could not be accepted as measure of the capacitances of the coatings, because the corresponding values of “n”, related to these constant phase elements occupy values close to 0.5. This value pre-determines the respective CPE, rather as diffusion elements. Consequently, intensive transfer of chemical species through the electric double layer occurs for both of the samples. Its presence is an indication of intensive surface processes on the surface of the samples.

The last time constants Q_3 which are ascribed to the diffusion processes in the bulk of the coatings have “n” - values close to 1. This fact can be explained by the diffusion processes in the pores of the coatings. The pores are hindered, as a consequence of hydrodynamic limitations, related to the geometry of the pores of the coatings. Other possible reasons for the hindered diffusion could be ascribed to partial obstruction either by Ce-oxide/hydroxide sediments, or to insoluble corrosion products.

4. Surface morphologic observations of the coatings by AFM

4.1. Topographic surface observations

Figure 52 shows 2D- topographic images of the samples, obtained by AFM.

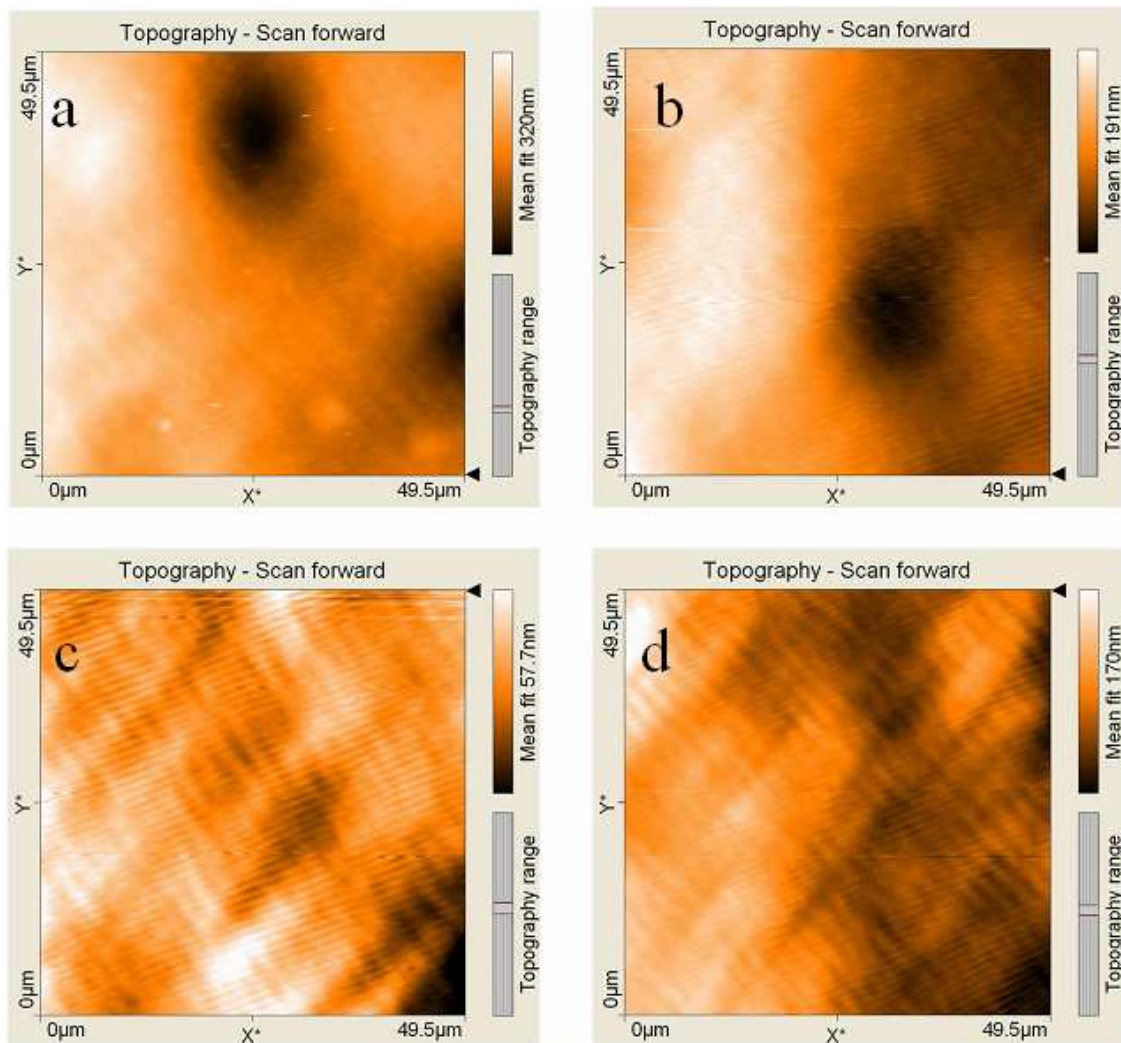


Figure 52. Topographic images of the samples, obtained by AFM.

a – sample A6; b – sample B1; c – sample H2; d – sample I2

The surfaces of the samples with addition of nano-particles look relatively smoother, and they do not follow the laminar surface morphology of the metal plates. It is indirect evidence that the hybrid nano-composite primer coatings are thick enough to not follow the morphology of the metal plates. This difference could be explained, having

into account the technological difference between the hybrid and the hybrid nano-composite primer coatings deposition. The addition of nano-particles as reinforcing phase, leads to change of the surface morphology of the respective coatings. Consequently, the addition of nano-particles, leads to their agglomeration, and after their deposition the coating surface does not repeat this of the metal plate.

Figure 53 shows the corresponding 3-D images of the samples surface at different magnification.

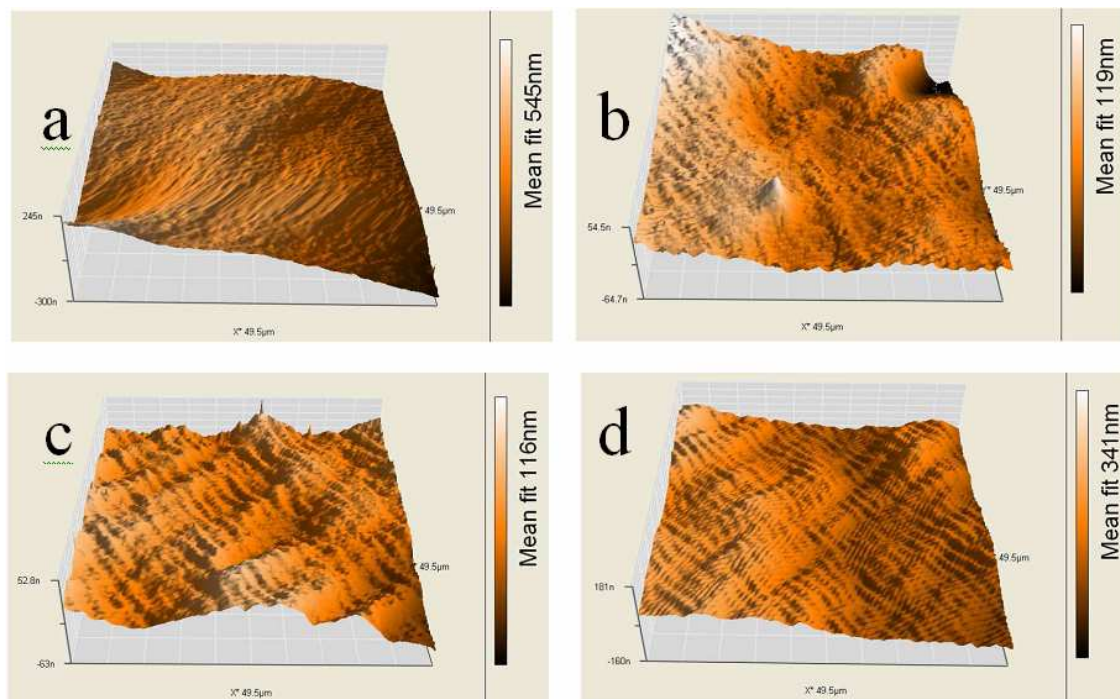


Figure 53. 3-D. images of the samples, obtained by AFM.

a – sample A6; b – sample B1; c – sample H2; d – sample I2

4.2. Quantitative evaluation of the surface roughness

Table 14 summarizes the quantitative data of the determined sample's roughness.

Table 14. Values of the sample's roughness

SAMPLE	CLA6		CLB1		CLH2		CLI2	
ROUGHNESS VALUE	Name	Value	Name	Value	Name	Value	Name	Value
	Area	2.459nm ²	Area	2.459nm ²	Area	2.459nm ²	Area	2.459nm ²
	Sa	50.292nm	Sa	48.069nm	Sa	17.124nm	Sa	28.194nm
	Sq	62.813nm	Sq	52.728nm	Sq	26.503nm	Sq	38.653nm
	Sy	448.98nm	Sy	211.71nm	Sy	335.88nm	Sy	423.63nm
	Sp	204.15nm	Sp	105.11nm	Sp	234.82nm	Sp	311.71nm
	Sv	-244.83nm	Sv	-106.6nm	Sv	-101.06nm	Sv	-111.93nm
	Sm	212.32pm	Sm	212.13pm	Sm	211.53pm	Sm	209.79pm

After detailed comparative analysis of the data for various parameters of the primer coatings, such as: their thickness (see section 1.1 and 1.2 in the Experimental part), their durability (see Tables from 3 to 13), their capacitance ($Q_{\text{coat+oxy}}$) and finally – the roughness parameters of the coatings (see Table 14) some interesting dependencies were discovered.

The samples which possess lower peak valley possess higher durability. The highest durability (125 days) belongs to the sample B1 with $S_y = 211,71$ nm. For comparison, the most rough primer coatings (I2 and A6 with $S_y = 423,63$ nm and 448,98 nm, respectively) reveal relatively lower durability. The sample H2 represents exclusion. It should be more durable than the sample A6 because the roughness of the former is lower than of the latter. In addition, the thickness of H2 is two times higher than this of A6. This phenomenon conform the concept proposed from Zheludkevich et. al.[41] regarding the gradual release of inhibitor when it is incorporated in nanoparticles. In addition, we can accept that the nanoparticles could serve as reinforcing phase to the hybrid matrix. This assumption is confirmed by M. Zheludkevich [21] who emphasises the superior properties of hybrid nanocomposite coatings, compared to the hybrid coatings. In this context, the present research work completed conforms the images describes in the theoretical part (point 1.6). The roughness mean values (see S_m values in Table 14) are almost equals, which means that the areas occupied by the mounts and the valleys are relatively equally distributed, despite the differences of their morphologies, as described above.

The values of capacitances ($Q_{\text{coat+oxy}}$) of the hybrid nanocomposites are relatively twice higher than these of hybrid coatings. Simultaneously the corresponding values of $R_{\text{coat+oxy}}$ are twice lower for the former case. These relations are rather connected to the thicknesses at the respective samples, because the thickness of the latter cases, are almost twice higher than the former. This relationship looks logical because the capacitance of the coatings is related to their thickness.

Principally, it should be expected that the capacitance of the coatings is also related to their roughness, because it predetermines the exposed to the electrolyte surface area. The analysis of the results obtained has not confirmed this expectation. The values of S_y are mainly randomizing distributed, while the S_m values are almost equal.

From the all experiments carried out and AFM observations described above we could be concluded that the electrochemical parameters $R_{\text{coat+oxy}}$ and $Q_{\text{coat+oxy}}$ are in close dependence predominantly from the coating thickness, and not so significantly influenced by their roughness and surface topology characteristics of the coatings.

V. CONCLUCIONS

The integral analysis of the experimental data leads to the following conclusions:

1. It was established that both of the coatings possess well expressed barrier ability. The values of the Ohmic resistance of the coatings are in the range of $1-10\text{M}\Omega\cdot\text{cm}^2$. The barrier ability of the coatings deteriorates with increasing of CeCl_3 content from 2 to 4%.

2. The described above detrimental effect of the increased quantity of CeCl_3 is expressed over the barrier ability as well. For the sample CIH2 with 2% of the inhibitor the coating's breakdown was observed after 79 days, while for the sample CII2 with 4% of CeCl_3 addition, it was established after 63 days of durability test procedure.

3. It was established that the values of the Ohmic resistance passes through a maximum, during the exposure of the samples to the corrosive medium. Probable reason for the appearance of these maxima is the presence of two controversial tendencies: a-Blocking of the pores by the insoluble corrosion products and b-Appearance of defects in the oxide layer under the cracks and ruptures of the coating.

4. When the CeCl_3 inhibitor is introduced directly in the hybrid matrix its durability is worse in comparison to the primer coating with preliminary impregnated nano-particles.

5. When the inhibitor is incorporated into the porous nano-particles, and afterwards the obtained systems are introduced into the hybrid matrix, the corrosion protective ability changes significantly. For pre-treatment with 2% CeCl_3 preliminary impregnated into 8% Al_2O_3 nano-particles (CIA6), its durability was up to 3000 hours of exposure, while pre-treatments with direct addition of the inhibitor, revealed lower durability.

6. The Nyquist plots of both pre-treatments, prepared by addition of CeCl_3 are consisted of deformed semi-circle, and long right line, with slope equal to 0.78 – 0.90, at the low frequency part of the spectra. The corrosion behaviour for this kind of pre-treatments passes to the diffusion limitations, and is deviates from the ideal Fick's law.

7. Numerical values for the properties of the pre-treatments have been obtained by fitting procedure of the spectra to appropriated equivalent circuits. In addition the development of these parameters within the exposure time was followed.

8. It was established, that the diffusion of species trough the coatings is strongly hindered, which could be ascribed to the action of the inhibitor used.

9. It was found that generally, the hybrid nanocomposite primer coatings possess better behaviour in corrosive medium when they are compared with ones (with corresponding additions of inhibitor), despite the twice lower thickness of the latter. Having in account this fact it is expectable that the hybrid nanocomposite should have much superior performance when they are compared with equal thickness with the respective hybrid coatings.

VI. REFERENCES

- [1]. J. Davis, ASM International. **“Corrosion: Understanding the Basics”** *American Technical Publishers Ltd, Materials Park, Ohio, (2000) p. 6-10*
- [2]. Frederico M. Mazzolani **“Aluminium alloy structures”** *E& FN SPON ed. Second edition (1985) pp. 5 – 25*
- [3]. http://www.substech.com/dokuwiki/doku.php?id=classification_of_aluminum_alloys
- [4]. V. Kozhukharov, S. Kozhukharov, G. Tsaneva, J. Gerwann, M. Schem, T. Schmidt, M. Veith. **“Investigation on the corrosion protection ability of nanocomposite hybrid coatings”** *Impedance Contributions Online 5 (2007) P-1 – P2-16, access via <http://accessimpedance.iusi.bas.bg>*
- [5]. L. Palomino, I. V. Aoki , H.G. de Melo **“Microstructural and Electrochemical characterization of Ce conversion layers formed on Al alloy 2024-T3 covered with Cu-rich smut”** *Electrochim. Acta 51 (2006) 5943-5953*
- [6]. M. Bethencourt, F. J. Botana, M. J. Cano, M. Marcos, J. M. S’anchez-Amaya, L. Gonz’alez-Rovira **“Behaviour of the alloy AA2017 in aqueous solutions of NaCl. Part I: Corrosion mechanisms”** *Corrosion Science 51(2009) 518 – 524*
- [7]. V. Kozhukharov, G. Tsaneva, S. Kozhukharov, J. Gerwann, M. Schem, T. Schmidt, M. Veith **“Corrosion protection properties of nanocomposite hybrid coatings with zirconia and ceria”** *Bulgarian Chemical Communications 78 (2007) 23 - 29*
- [8]. N. C. Rosero Navarro, M. Curioni, R. Bingham, A. Dur’an, M. Aparicio, R. A. Cotti, G. E. Thompson **“Electrochemical techniques for practical evaluation of corrosion inhibitor effectiveness. Performance of cerium nitrate as corrosion inhibitor for AA2024-T3 alloy”** *Corrosion science 52 (2010) 3356 – 3366*
- [9]. J.H. Osborne, *Prog. Org. Coat.* **41** (4) (2001) 280–286.
- [10]. A. Hughes, R. Taylor, B. Hinton, *Surf. Interface Anal.* **25** (4) (1998) 223–234
- [11]. W.R. McGovern, P. Schmutz, R.G. Buchheit, R.L. McCreery, *J. Electrochem. Soc.* **147** (12) (2000) 4494–4501
- [12]. M. Schem, T. Schmidt, H. Caparotti, M. Wittmar, M. Veith, **“Corrosion inhibiting cerium compounds for chromium-free corrosion protective coatings on AA 2024”** *Proceed. “Eurocorr. 2007”, Freiburg - Germany*

- [13]. G. Tsaneva, V. Kozhukharov, S. Kozhukharova, M. Ivanova, J. Gerwann, M. Schem, T. Schmidt, “**Functional nanocomposite coatings for corrosion protection of aluminium alloy and steel**”, *Journal of the University of Chemical Technologies and Metallurgy* 43 (2) (2008) 231 - 238
- [14]. A. S. Hamdy, D.P. Butt “**Environmentally compliant silica conversion coatings prepared by sol –gel method for aluminum alloys**” *Surface & Coatings Technology* 201 (2006) 401 – 407
- [15]. R. Petrucci & W. Harwood “**Química general. Principios y aplicaciones modernas**” ISBN: 84-8322-043-1 editor Prentice Hall Iberia, S.LR. 1998 page 496
- [16]. S. Kozukharov “**Relationship between the conditions of preparation by the sol-gel route and the properties of the obtained product**” *Journal of the University of Chemical Technologies and Metallurgy* 44 (2) (2009) 143-150
- [17]. E. C. Cordoncillo “**Prreparación de vidrios basados en una matriz de silice con procesado sol-gel, aplicación a la obtención de nuevos vidrios ópticos de cinc y cadmio**” *Doctoral thesis Castellon (Spain) 1995, pp. 16*
- [18]. H. Dislish, *J. Non. Cryst Sol.* 73 (1985) 599-612
- [19]. H. K. Schmidt, E. Geiter, M. Menning, H. Krug, C. Becker, R. Winkler, *J. Sol. Gel. Sci. Tech.*, 13 (1998) 397-404
- [20]. J. Mackenzie, E. Bescher, *J. Sol. Gel. Sci. Tech.* 19 (2000) 23-29
- [21]. M. L. Zheludkevich, I. M Salvado, M. G. S. Ferreira “**Sol–gel coatings for corrosion protection of metals**” *J. Mater. Chem.*, 15, (2005) 5099–5111
- [22]. K. Haas, K. Rose “**Hybrid inorganic/organic polymers with nanoscale building blocks: precursors, processing**” *Rev. Adv. Mater. Sci.* 5 (2003) 47–52
- [23]. P.E. López, J. B. Carda Castelló, E. C. Cordoncillo “**Esmaltes y pigmentos Cerámicos**” *Editor: Faenza Editrice Iberica (Castellon), 2001, pp. 255*
- [24]. B. Samuneva, V. Kozhukharov, C. Trapalis “**Sol-gel processing of titanium-containing thin coatings Part I Preparation and structure**” *Jour. Mat. Sci.* 28 (9), (1993) 2353 – 2360
- [25]. V. Palavinel, Y. Huang, and W. van Ooij “**Effects of addition of corrosion inhibitors to silane films on the performance of AA2024-T3 in 0.5 M NaCl solutioin**” *Progress in Organic Coatings* 53 (2005) 153 – 168

- [26]. A. Frignani, F. Zucchi, G. TrabANELLI and V. Grassi, **“Protective action towards aluminium corrosion by silanes with long aliphatic chain”** *Corrosion Science* **48** (2006) 2258 - 2273
- [27]. P. Laibinis, G. Whitesides, D. Allara, Y-T. Tao, A. Parkin and R. Nuzzo, *J. Am. Chem. Soc.* **113** (1991) 7152
- [28]. J. Malzbender and G. de With, *Adv. Eng. Mater.* **4** (2002) 296 – 302
- [29]. F. Zamborini and R. Crooks, *Langmuir* **14** (1998) 3279
- [30]. M. Zheludkevich, R. Serra, M. Montemor and M. Ferreira., **“Oxide nanoparticle reservoirs for storage and prolonged release of the corrosion inhibitors”** *Electrochem. Commun.* **7** (2005) 836
- [31]. N. Rosero-Navarro, S. Pellice, Y. Castro, M. Aparicio and A. Durán **“Improved corrosion resistance of AA2024 alloys through hybrid organic-inorganic sol-gel coatings produced from sols with controlled polymerisation”** *Surface & Coatings Technology* **203** (2009) 1897–1903
- [32]. G. Jennings, T. Yong, J. Munro, P. Laibinis, *Jour. Am. Chem. Soc.* **125** (2003) 2950
- [33]. Y. Ma, C. Yang, S. Chen, L. Jiao, X. Huang, G. Li and L. Luo, *Electrochim Acta* **48** (2003) 4277
- [34]. S. Ono, H. Tsuge, Y. Nishi, S. Hirano, *J. Sol-Gel Sci. Tech.* **29** (2004) 147
- [35]. R. S. Witt, *Jour. Electrochem. Soc.* **114** (1987) pp. 848 - 855
- [36]. N. Voevodin, J. Kurdziel and R. Mantz **“Corrosion protection for aerospace aluminum alloys by Modified Self-assembled Nano-Phase (MNSNAP) sol-gel”** *Surface and Coating Technologies* **201** (2006) 1080 - 1084
- [37]. N. Voevodin, N. Grebush, W. Soto, F. Arnold and M. Donley **“Potentiodynamic evaluation of Sol-Gel Coatings with inorganic inhibitors”** *Surf. Coat. Tech.* **140** (2001) 24 – 28
- [38]. A. Vregdenhil, V. Balbyshev, M. Donley, *Journal of Coating Technology* **73**(2001) 35
- [39]. E. Matter, S. Kozhukharov, M. Machkova, V. Kozhukharov **“Influence of the interactions between the corrosion inhibitor and nano-containers over the corrosion protective capability of hybrid nano-composite pre-treatments”** *Proceed. “Chemical Technologies Biotechnologies and Food technologies” Tech. University Rousse, Volume 48, Book 9 (2009) 19-23*

- [40]. M. Zheludkevich, R. Serra, M. Montemor and M. Ferreira., **“Oxide nanoparticle reservoirs for storage and prolonged release of the corrosion inhibitors”** *Electrochem. Commun.* **7** (2005) 836
- [41]. EU Directive 2002/95/EC **“Restriction of Hazardous Substances in Electrical and Electronic Equipment”** (RoHS directive 2002), via www.broadcom.com/docs/ & www.chem.agilent.com/
- [42]. Directive 2004/107/EC of the European Parliament and of the Council of 15 December 2004 relating to arsenic, cadmium, mercury, nickel and polycyclic aromatic hydrocarbons in ambient air. Official Journal of the European Communities L 23, 26.1.2005, p. 3–16, Special edition in Bulgarian: Chapter 15 Volume 13 P. 124 – 137
- [43]. K. Yasakau, M. Zheludkevich, S. Lamaka, and M. G. S. Ferreira **“Mechanism of Corrosion Inhibition of AA2024 by Rare-Earth Compounds”** *J. Phys. Chem. B*, **110** (2006) 5515 -5528
- [44]. S. Lamaka, M. Zheludkevich, K. Yasakau, R. Serra, S. Poznyak and M. Ferreira **“Nanoporous titania interlayer as reservoir of corrosion inhibitors for coatings with self-healing ability”** *Progress in Organic Coatings* **58** (2007) 127– 135
- [45]. N. Voevodin, N. Grebush, W. Soto, F. Arnold and M. Donley **“Potentiodynamic evaluation of Sol-Gel Coatings with inorganic inhibitors”** *Surf. Coat. Tech.* **140** (2001) 24 – 28
- [46]. A. S. Hamdy and A. M. Beccaria, **“Effect of surface preparation prior to cerium pre-treatment on the corrosion protection performance of aluminum composites”** *J. Appl. Electrochem.* **35**, (2005), 473–478
- [47]. M. L. Zheludkevich, R. Serra, M. F. Montemor, K. A. Yasakau I. M. Miranda Salvado, M. G. S. Ferreira **“Nanostructured sol-gel coatings doped with cerium nitrate as pre-treatments for AA2024-T3 Corrosion protection performance”** *Electrochimica Acta* **51** (2005) 208 - 217
- [48]. A. Aldykiewicz, A. Davenport, H. Issacs, *J. Electrochem. Soc.* **143**(1996) 147 –155
- [49]. P. Suegama, H. de Melo, A. Benedetti, I. Aoki, **“Influence of cerium (IV) ions on the mechanism of organosilane polymerization and on the improvement of its barrier properties”** *Electrochimica Acta* **54** (2009) 2655–2662

- [50]. G.Jonschker, S.Langenfeld and H.Schmidt, **“Method for protecting a metallic substrate against corrosion”** *US Patent No. 6,403,164* (2002)
- [51]. L. Stephenson, A. Kumar **“Technology Demonstration of Self-Healing Coatings for In-Place Management of Lead-Based Paint Hazards”** *US Army Corporation of Engineers-Engineer Research and Development Center; December 2003, p. 5- 6*
- [52]. Z. Liu, Z. Jin, X. Liu, Y.Fu and G. Liu, **“Fabrication of ordered TiO₂ porous Thin Film by Sol-Dipping PS Template Method”** *J. Sol-Gel Science & Technology* **38** (2006) 73 – 78
- [53]. F. Scholtz, **“Electroanalytical methods. Theory and Practice”** Ed. *“Laboratory of knowledge”- 2006 Moscow (Russia), pages 19-20 (In Russian)*
- [54]. Budevski E, Staikov G, Lorenz WJ **“Electrochemical phase formation and Growth”**, VCH, Weinheim (1996)
- [55]. <http://www.ecochemie.nl/export/Homepages/downloads/Applicationnotes/Appl.011>
- [56]. Joao Fernandez **“Brief lecture course on Impedance Spectroscopy”** *Workshop – 6-7 of November; 2008 Lisbon (Portugal), page 32*
- [57]. S. Kozhukharov, G. Tsaneva, V. Kozhukharov, J. Gerwann, M. Schem, T. Schmidt, M. Veith **“Corrosion protection properties of composite hybrid coatings with involved nanoparticles of Zirconia and Ceria”** *Jour. of the Univ. of Chem. Tech. Met.* **43, 1** (2008) 73-80
- [58]. G.Jonschker, S.Langenfeld and H.Schmidt, **“Method for protecting a metallic substrate against corrosion”** *US Patent No. 6,403,164* (2002)
- [59]. M.Schem, T. Schmidt, H. Caparrotti, M. Aslan, M. Veith, M. Wittmar, *Proc. Eurocorr 2008, paper 1034, Edinburgh, UK, 7-11 Sept, 2008.*
- [60]. D. Wang, G.P. Bierwagen **“Sol-gel coatings on metals for corrosion protection”** *Progress in Organic Coatings* **64** (2009) 327-338
- [61]. Choong-Soo Chi, Y. Jeong, Hong-Joo Ahn, Jong-Ho Lee, Jung-Gu Kim, Jun-Hee Lee, Kyung-Wook Jang and Han-Jun Oh **“Transition of hydrated oxide layer for aluminum electrolytic capacitors”** *Materials Science and Engineering: A* **449-451**, (2007), 314-317
- [62]. M.L. Zheludkevich, R.Serra, M.F. Montemor, K.A.Yasakau, I.M. Miranda Salvado, M.G.S. Ferreira; *Electrochimica Acta*, **51, 2** (2005) 208-217

- [63]. M.L. Zheludkevich, M.F. Montemor, I.M. Salvado, M.G.S. Ferreira,
“**Electrochemistry Communications**” 7, (2005) 836-840